NASA TM X-439

TECHNICAL MEMORANDUM

X-439

THE EFFECT OF AIR BLEED ON THE HEAT TRANSFER AND PRESSURE DISTRIBUTION ON 30° CONICAL FLARES AT A MACH NUMBER OF 6.8

By Davis H. Crawford

Langley Research Center
Langley Field, Va.

NATIONAL AERONAUTICS AND SPACE ADMINISTRATION

WASHINGTON March 1961

NATIONAL AERONAUTICS AND SPACE ADMINISTRATION

TECHNICAL MEMORANDUM X-439

THE EFFECT OF AIR BLEED ON THE HEAT TRANSFER AND PRESSURE DISTRIBUTION ON 30° CONICAL FLARES AT A MACH NUMBER OF 6.8*

By Davis H. Crawford

SUMMARY

The effect of a boundary-layer bleed at the start of a 30° half-angle flare upon the shape of the flow boundaries, the pressure distribution on the flare, and the heat transfer to the flare was studied at a Mach number of 6.8. The forebody was an ogive cylinder. Test Reynolds numbers, based on forebody length, ranged from 1×10^6 to 7.4×10^6. Schlieren photographs showed the effect produced upon the flow boundaries by varying the dimensions of the bleed in both the radial and axial directions and by blunting the lip at the leading edge of the flare. The heat transfer and pressure distribution on the flare were correlated with the shape and nature of the flow boundaries.

INTRODUCTION

Flares are often used as a device to stabilize missiles. They could also be used to control the drag of reentry vehicles. A factor to be considered in their use, however, is the influence of separation upon the effectiveness of the flare. The extent of separation induced by unfavorable pressure gradients transmitted forward by steps, wedges, and flares has been widely investigated. (See refs. 1 to 8.) It has been shown that separation ahead of a 30° half-angle flare is reduced by an increase in Reynolds number when the separated boundary is transitional, and that separation becomes almost nonexistent when transition occurs on the body ahead of separation (refs. 7 and 8). The extent of separation ahead of a flare may alter the stability derivatives of the vehicle, the drag produced by the flare, and the heat transfer to the flare in high-speed flight (refs. 7 to 15).

*Title, Unclassified.

One possible method of controlling the extent of separation at high altitudes and low Reynolds numbers is the incorporation of a boundary-layer bleed at the start of the flare (refs. 8 and 16). Regulation of the bleed would provide limited programing of the drag of a reentry vehicle. Peak heating effects, characteristic of the reattachment of the boundary layer, could be minimized by control of the position of reattachment. At lower altitudes and higher Reynolds numbers, where the separation ahead of the flare is negligible and the boundary layer is turbulent over the entire flare, the bleed could reduce the heat transfer to the flare by bleeding off the turbulent boundary layer and allowing the start of a new laminar boundary layer on the foremost surface of the flare.

The purpose of the present investigation was to study the effect of a boundary-layer bleed at the start of a flare upon the shape of the flow boundaries set up by an ogive-cylinder body with fineness ratio of approximately 10 followed by a 30° half-angle flare and upon the heat transfer and pressure distributions over the surface of the flare. Models were tested at a Mach number of approximately 6.8 and Reynolds numbers ranging from 1×10^6 to 7.4×10^6 based on free-stream conditions ahead of the model and on the forebody length. This range of Reynolds numbers was sufficient to allow testing with laminar, transitional, and turbulent separated boundary layers. The experimental results were compared with calculated results by using a combination of schlieren data, two-dimensional and three-dimensional compressible-flow theories, and laminar and turbulent flat-plate heat-transfer theories.

SYMBOLS

c_{f_o} local skin friction at beginning of interaction

$$\tilde{c}_f \equiv \frac{\left(c_{f_o}\right)}{\left(c_{f_o}\right)_{R_{x_o}=10^6}}$$

C_{Dp} pressure drag coefficient of flare $C_{Dp} = \int_0^1 C_p \, d\left(\frac{r}{R}\right)^2$

C_p local pressure coefficient

d diameter of entrance of flare

D	base diameter of flare
l	surface distance from leading edge of flare to station
M	Mach number
N_{Pr}	Prandtl number
N_{St}	Stanton number based on stream conditions ahead of model
$\bar{N}_{St}$	average Stanton number on surface of flare
p	local pressure necessary to separate boundary layer
p_o	local pressure at beginning of interaction
r	local radius of body and flare
R	radius of flare base
R_L	Reynolds number based on stream conditions ahead of the model and on forebody length
R_{x_o}	Reynolds number based on local conditions at beginning of interaction
s	surface distance from base of flare to measuring station locations
S	surface distance from base to leading edge of flare
x	axial dimension of flare bleed gap
X	axial coordinate used on forebody
y	radial dimension of flare bleed gap
θ	angle of separation near the start of separation

APPARATUS

Tunnel

The present investigation was conducted in the Langley 11-inch hypersonic tunnel described in references 17 and 18. Air is stored at

50 atmospheres' pressure and is released to the settling chamber and nozzle through an adjustable pressure-regulating valve and an air heater with tube resistance elements of nickel-chromium alloy. (This air heater replaces the storage heater described in refs. 17 and 18.) A two-dimensional nozzle constructed of Invar and designed for a Mach number of 7 was used for this investigation.

Models

The basic shape studied in this investigation was an ogive-cylinder forebody with a 30° half-angle tail flare. A view of the assembled model is shown in figure 1. Two forebodies of different diameters were used in the tests to allow control of the radial dimension of the flare bleed gap. Both forebodies had Karman minimum-drag nose shapes of fineness ratio 5 modified by placing a 10° half-angle cone, tangent to the nose, at the tip. The smaller ogive nose was followed by a 1.5-inch-diameter cylinder 5 diameters in length to complete the forebody and is designated forebody I. Forebody II was obtained by increasing the ogive-nose dimensions by 20 percent, but was followed by a cylinder shorter than the cylinder of forebody I so that the overall length was 15.474 inches for each forebody. These forebodies could be positioned at different distances ahead of the flare to allow control of the axial dimension of the flare bleed gap. The forebodies were constructed of solid steel, and neither temperature nor pressure data were taken on their surfaces.

Three different flares were used in the tests as shown in figure 2. All flares had base diameters of 4.64 inches and were 0.10 inch thick. One of the flares had a sharp leading edge and was 1.80 inches in diameter at the entrance, and the other two had leading edges blunted to a 0.05-inch radius and had inside diameters at their entrances of 1.80 inches and 2.10 inches. The parts of the flare were machined of SAE 1020 carbon steel, and all permanent assemblies of parts were effected by silver solder. All the test configurations used in this investigation were assembled by combining the flares and forebodies in different positions with regard to the leading edge of the flare.

Test Conditions

For these tests it was considered important to vary the Reynolds number over a wide range. The Reynolds number was controlled primarily through the stagnation pressure, but was affected somewhat by the incidental variation in stagnation temperature between runs. The tunnel stagnation pressures used were as low as 5.2 atmospheres and as high as 41 atmospheres, and the stagnation temperatures ranged from about 1,050° R to about 1,190° R. Tunnel calibrations have indicated

a Mach number of 6.86 ± 0.04 in the central core of uniform flow at a stagnation pressure of 30 atmospheres and at a time 60 seconds after the start. The central core of uniform flow measures about $6\frac{1}{2}$ inches in the vertical direction and about 6 inches in the horizontal direction. However, the tunnel Mach number varies with the tunnel stagnation pressure and with the time during the run from about 6.5 near the start of the low-pressure runs to nearly 6.9 for the high-pressure runs at about 60 seconds after the start. Test Reynolds numbers based on free-stream conditions and forebody length ranged from about 1.0×10^6 to 7.4×10^6.

L
1
2
2
1

Instrumentation

Thermocouples and pressure orifices were installed along three rays 90° apart on the surface of the flare. The thermocouples were of No. 30 gage (0.010-inch-diameter) chromel-alumel wire and were located at identical stations with respect to the trailing edge. These thermocouples were soldered into holes in the model skin so that their effective measuring junctions were located on the inner surface. Since the skirts of these flares were of varying lengths, the sharp and blunt flares with entrances 1.80 inches in inside diameter had 9 and 10 temperature stations, respectively, and the blunt flare with an entrance 2.10 inches in inside diameter had 8 temperature stations. The sharp and blunt flares with entrances 1.80 inches in inside diameter were instrumented with an internal pressure orifice (fig. 1) and two external pressure orifices (fig. 2). Both the external and internal orifices were 0.040 inch in inside diameter. The blunt flare with an entrance 2.10 inches in inside diameter had five external pressure orifices as well as the internal orifice. The internal orifice of this flare was 0.100 inch in inside diameter while the external orifices were 0.040 inch in inside diameter.

The temperature measurements included tunnel stagnation temperature and flare skin temperature. The stagnation temperature was measured by shielded thermocouples distributed at various stations in the settling chamber. These temperatures were recorded by 12-channel self-balancing potentiometers. The temperatures sensed by the thermocouples in the flare skin were recorded by the same method for some of the tests, but were recorded both by potentiometers and by fast-response oscillographs for other tests. The experimental results from the two types of records were found to agree closely, and the oscillograph records were easier to use. Since in most cases the stations in one ray were connected to potentiometer recorders and the stations in the other ray were connected to oscillograph recorders, the oscillograph data were complete and were used alone in these cases. One stagnation thermocouple was read on an

oscillograph to aid in the determination of zero time and to determine qualitatively the variation of stagnation temperature with time near the start of the run.

Flare pressures were recorded on film by the evacuated-capsule instruments described in reference 17. When possible, pressure cells were chosen to give near full-scale deflection for the pressure recorded. The stagnation pressure was recorded manually from the indication of a high-accuracy Bourdon gage.

The shape and the nature of the flow around the model were obtained from a schlieren system which had a single-pass vertical-Z light path with a horizontal knife edge. This system may be arranged either to project the image on a screen for visual observation or to record the image on still or motion-picture film. The light source for the still photographs was a spark-fired mercury-vapor lamp which was operated for a light duration of about 3 microseconds. The same lamp was operated continuously with a lower intensity for the motion-picture records. The maximum speed of these records was about 7,000 frames per second.

L 1 2 2 1

TEMPERATURE-DATA REDUCTION

The heat transfer to the flares was determined by a transient method. This method consisted of suddenly subjecting the model to the test flow conditions and determining the time rate of change of model temperature near the start of the test. The method has been outlined in detail in reference 6 and has the advantage of reducing or eliminating any possible correction for conduction in the model skin. Also, the constant-wall-temperature theoretical solutions may be compared with the experimental results with more validity. The experimental heat-transfer results are presented in the form of the nondimensional parameter $N_{St}\sqrt{R_L}$, where the flow conditions used are the free-stream conditions ahead of the model and the characteristic length used is the length of the forebody.

Because of the uncertainty involved in a priori assumptions of laminar, transitional, or turbulent boundary-layer flow for the choice of recovery factor, a constant value for recovery factor $\sqrt{N_{Pr}}$ of 0.88, based on local stream conditions, was used for all results. This high value was chosen because most flow after reattachment was transitional or turbulent and also because the stream temperature was low enough (150° R) to produce a somewhat high Prandtl number (0.77) in the case of the heat transfer under the separated laminar boundary. The greatest error in the calculation of the heat-transfer coefficient caused by this choice of recovery factor occurred when separation was prevented by a

large gap. These results could be as much as 6 percent lower than the values which would have been calculated with a more realistic recovery factor of about 0.84 for this case.

RESULTS AND DISCUSSION

Shape and Nature of the Separated Boundary Layer

L-1221 Observations of the shape and nature of the flow over these test configurations show trends similar to those for similar body shapes in references 7 and 8 and also similar to those for other body shapes in references 1 to 6. The flow separated from the surface of the body ahead of the flare when the pressure rise caused by the shock at the start of the flare exceeded the maximum allowable for an attached boundary layer. The region of flow separation varied in size from one in which the boundary separated slightly ahead of the constant-diameter cylindrical segment of the body and attached at the trailing edge of the flare to one in which no separation ahead of the flare was observed.

A qualitative idea of the effect of the different boundary-layer bleeds as well as the effect of the different test Reynolds numbers upon the flow is shown in the schlieren photographs of figures 3 and 4. The horizontal rows of photographs show the change produced by different flare-bleed gaps at approximately the same Reynolds numbers. In general, the size of the flare-bleed gap is increasing from left to right. In three instances the flow over the flare with a certain bleed gap is compared with the flow over the flare with the same bleed gap but with the flare plugged so that no air is removed by the bleed gap. The vertical rows of photographs show the effect of Reynolds number upon the separated boundaries for flares with the same bleed gap.

The effect of Reynolds number upon the separated boundary over the model with no flare bleed (fig. 3(a)) has been previously described in references 7 and 8. At low Reynolds numbers, when the flow is entirely laminar in the region of separation, the start of separation moves forward slightly with increasing Reynolds number as is expected for this case (ref. 2). As the Reynolds number increases and the boundary layer over the separated region becomes transitional, the position of the start of separation moves back toward the flare. When the Reynolds number is high enough to cause the start of transition ahead of separation, the region of separation is reduced to the barely perceptible separation bubble seen in figure 3(a) with $R_L = 6.8 \times 10^6$.

The schlieren movies showed a varying amount of unsteady flow as a result of the separated regions. In some tests there was a rapid

small-amplitude fluctuation of the position of the start of separation, which was amplified to a larger amplitude fluctuation of the position of reattachment. In other tests the separated region was seen to collapse for an instant at random intervals of time. The free-stream Reynolds number was varied slowly for some of these tests, and the tendency to collapse was seen over the entire Reynolds number range. There is a strong possibility that the violent unsteadiness which led to complete collapse of the separated boundary was caused at least in part by unsteadiness of the flow in the tunnel. It is likely that this unsteadiness was coupled with the movement of transition on the separated boundary.

Along with the fluctuation of the position and shape of the separated boundary, a higher-frequency fluctuation is apparent in the spark schlieren pictures of figures 3 and 4, which were taken with a light duration of about 3 microseconds. This higher-frequency fluctuation shows up as a waviness of the separated boundary and is similar to that observed in the flow over a spiked-nose hemisphere-cylinder in reference 6. In neither study is this higher-frequency fluctuation seen in the individual frames of schlieren movies taken at a maximum of 7,000 frames per second. In reference 19, Stollery, Maull, and Belcher reported that a high-frequency unsteady flow was seen on a spiked-nose blunt body at $M = 6.8$. In that particular investigation eight sparks could be obtained at 10-microsecond intervals by means of a multiple-spark source. The frequency of fluctuation was determined to be about 25,000 cycles per second. Frequencies seen on similar bodies have been reported by Mair to be 6,000 cycles per second at $M = 1.96$ (ref. 20), and by Bogdonoff and Vas to be about 10^4 cycles per second at $M = 14$ in helium (ref. 21).

Before discussing the effect of the flare bleed upon the nature of the separated region ahead of the flare, the results of the internal-pressure measurements of the flare should be mentioned. For part of the tests the lag time was a serious problem, but the value of the internal flare pressure was indicated to be roughly one-half the free-stream value. This is somewhat higher than the expected base pressure (refs. 22 to 25), but the pressure inside the flare may reasonably be expected to be above the base pressure because of the shock loss to the high-energy air entering the flare. The base pressure may be affected slightly by the pressure transmitted forward along the sting mount. Some of the measured internal flare pressures were approximately double the free-stream pressure. These results occurred during tests at the highest Reynolds number with the largest boundary-layer bleed sizes ($R_L \approx 7 \times 10^6$: fig. 3(e) for sharp-lip flare; figs. 4(f), 4(g), and 4(h) for blunt-lip flare). It is probable that the shock loss of the high-energy air near the entrance of the flare caused a

choking of the exit orifices of the flare in these cases. The flow boundary just ahead of the flare in these cases appears to have been affected by this additional internal flare pressure in that the separation is slightly more extensive and the location of reattachment has been displaced slightly.

The effect of the changes in size and shape of the boundary-layer bleed gap upon the shape and extent of the separated region is strongly dependent upon the Reynolds number of the test. In the tests in figures 3 and 4 at high Reynolds numbers ($R_L \approx 7 \times 10^6$), the separated region was almost nonexistent for models with no gap; thus even when a small gap was present with a sharp lip, no apparent separation was visible. At intermediate Reynolds numbers ($R_L \approx 3.5 \times 10^6$), it appeared that the smallest axial bleed dimension (fig. 3(b)) had little effect upon the extent of separation, whereas with the smallest radial dimension (fig. 3(c)) the "dead air" region was completely swallowed. Here it appears that the radial dimension of the bleed has more effect upon the extent of separation than the axial dimension. At this Reynolds number the width of the radial gap was slightly larger than the laminar boundary-layer thickness at the start of the flare as determined by equation (14) of reference 26. At the two lowest Reynolds numbers ($R_L \approx 1.8 \times 10^6$ and $R_L \approx 1 \times 10^6$) the shape and extent of the separated region appeared little influenced by any of the sharp-lipped bleed configurations tested. At these Reynolds numbers the width of the radial gap was less than the laminar boundary-layer thickness at the start of the flare.

Schlieren movies showed that the unsteady characteristics of the separated boundary were less pronounced with the flare gap than with no gap. For some tests the flare was moved back and forth with respect to the forebody; that is, the size of the axial bleed gap was varied during the tests. The separated flow was steady with movement of the flare except at the instant when the gap became large enough to swallow the separation. At that instant the separation disappeared between frames taken at about 32 frames per second. It reappeared between frames as the gap was reduced in size. A slight hysteresis in this effect was seen in that before the separated boundary snapped into place the gap was reduced to a size smaller than the size which was necessary to again prevent separation.

Blunting the lip of the flare had an important effect upon the flow boundaries. The pressure rise caused by the blunt lip was transmitted forward and resulted in a thickening of the boundary layer even though the bleed was sufficiently large to prevent any extensive separation. This effect was observed even when the axial dimension of the bleed was several boundary-layer thicknesses (for example, fig. 4(h)),

and thus the pressure rise due to the strong shock standing off the blunt lip was transmitted forward through the subsonic part of the separated boundary layer. Larger radial boundary-layer bleeds ($y/D = 0.065$) were used with the blunt lip than with the sharp lip ($y/D = 0.032$). The largest bleeds (figs. 4(g) and 4(h)) were large enough to prevent extensive flow separation at the lowest test Reynolds number $\left(R_L \approx 1 \times 10^6\right)$. Thus it may be concluded that a larger boundary-layer bleed would have prevented separation ahead of the flare with the sharp leading edge at the lowest Reynolds number.

A rearward-facing step which causes a separated boundary ahead of a wedge or flare has been suggested in reference 3 as a means of reducing the extent of separation by allowing the boundary layer to gain more momentum and be better able to withstand the pressure rise at reattachment. An attempt to observe this effect on some of the configurations of this investigation resulted in the flow pictures shown in figures 3(f), 4(e), and 4(i) with the flow blocked in the flare. No attempt was made to measure heat transfer or pressure in the tests with the flow blocked in the flare, but the effects of the flow block upon the heat transfer and pressure distribution can be inferred from the changes in the shape of the flow boundaries. In comparing the flow boundaries for the models having no gap with the flow boundaries for the models having an effective depressed region, the shape of the flow boundaries is seen to differ slightly at the highest Reynolds number $\left(R_L \approx 7 \times 10^6\right)$, which was sufficiently high to prevent separation for the models with no gap, but at all lower Reynolds numbers $\left(R_L \approx 5 \times 10^6 \text{ and below}\right)$ the shape of the flow boundaries is essentially unchanged. Thus, in this particular application the rearward-facing step ahead of the flare caused negligible reduction in the extent of separation. Perhaps the failure of the step to reduce separation in this case is due to insufficient distance between the step and the flare.

L-1221

The effect of bleed dimensions and Reynolds number on the angle of flow separation is shown in figure 5, and their effect on the location of the reattachment point is shown in figure 6 for the sharp-lip flare. The dashed lines indicate regions where the shape of the faired curve is uncertain. The scatter of the data in figure 5 prevents any accurate quantitative conclusions, but the data of figure 6 again support the conclusion that the enlargement of the radial dimension of the boundary-layer bleed has more effect than the enlargement of the axial dimension.

The angle of separation as predicted by the wedge pressure result of a simple order-of-magnitude analysis of free interactions

$\left(\frac{\Delta p}{p_o} \sim \sqrt{\tilde{c}_f} \sim \left(R_{x_o}\right)^{-1/4}$ from ref. 1$\right)$ has been included in figure 5. The experimental values would not be expected to follow this theory except in general, since for the longest separation the start of separation occurs on the ogival nose and thus is moving in a region of Mach number gradient which includes some curvature of the surface.

Pressure Distribution on Flares

L-12211

Only two pressure orifices were installed in each of the flares with blunt leading edge and sharp leading edge which were used for the tests with radial dimensions of boundary-layer bleed of $y/D = 0$ and $y/D = 0.032$. The pressures recorded at these two stations are shown in figures 7 and 8. Measurements of pressure at only two stations, however, were inadequate to fair the pressure-distribution curves shown in these figures. The flare-pressure data from another model with no gap at the start of the flare, with the same forebody coordinates as the small forebody used in this investigation, but with a smaller base diameter (3.87 inches) was studied to obtain a more accurate idea of the correct shape of the pressure distribution. These data are shown in figure 9 and suggest the assumption that the shape of the curve for pressure plotted against $(r/R)^2$ in the region of reattachment is similar at different Reynolds numbers, and that a Reynolds number variation causes a relocation of this basic pressure distribution along with the relocation of reattachment. For want of a better method to determine the pressure distributions over the flares, it was assumed that the basic shape of the pressure distribution in the region of reattachment was not seriously altered by the use of a flare bleed. The accuracy of this assumption was tested in the only manner available. The shape of the curve in the reattachment region of figure 9 was compared with the shape seen on the blunt-lip flare in figure 8(a) in the case which had extensive separation ($L/D = 0.048$, $y/D = 0.065$). This comparison is probably the one which allows the widest probable divergence in the shape of the pressure distribution in the region of reattachment. Although these shapes do not agree exactly, it is felt that the errors introduced by the assumption of similar shapes of pressure distribution in the region of reattachment do not invalidate the conclusions based on this assumption.

The pressures just behind reattachment on the flare were calculated from the local free-stream properties of the airflow just ahead of separation in front of the flare and from the angles of the separated boundaries measured from the schlieren pictures. This was accomplished by determining the new stagnation pressure and Mach number behind the bow shock from the cone angle and by assuming all subsequent expansions and compressions to be two dimensional in nature. The expected shape

of the pressure distribution, the location of the position of reattachment, the calculated pressures after reattachment, and the two available measured pressures were used in fairing the curves of figures 7 and 8. Pressures were measured on the sharp-lip flare and on the blunt-lip flare with the smaller radial gap at the lowest Reynolds number $\left(R_L \approx 1.1 \times 10^6\right)$, but the lag errors for these data were so great as to invalidate the results. Lag was no problem in the case of the blunt-lip flare with the larger radial gap since pressure leads of a larger diameter were used.

A step in the pressure data on the blunt flare with the larger radial bleed gap $(y/D = 0.065)$ is clearly defined in figures 8(a), 8(b), 8(c), and 8(d). The reason for this step is clearly shown in the schlieren pictures of figures 4(f), 4(g), and 4(h). Even though this wide gap has prevented the extensive separation seen for a model with no gap and smaller gaps at low Reynolds numbers, a slight separation is caused by the pressure rise of the blunt lip, as has been previously mentioned. The shock from the start of this separation crosses the shock from the start of the flare in the neighborhood of the step in the pressure data. Transition ahead of separation has prevented laminar separation in front of the base of the forebody for the tests at the highest Reynolds number $\left(R_L \approx 7 \times 10^6\right)$, and has prevented the shock crossing seen at lower Reynolds numbers. Thus the lack of the step in the pressure data of figure 8(e) is expected. No shock crossing is seen in flow over flares with the smaller radial bleed gap $(y/D = 0.032)$; thus no similar step in the pressure data is expected in any of the tests of either flare with only two surface-pressure measurements.

L-1221

The flare pressure distributions of figures 7 and 8 were integrated to determine how the pressure drags were influenced by the various boundary-layer bleeds and Reynolds numbers and thus by the varying shape of the separated boundaries. Since the local pressure coefficients were plotted against $(r/R)^2$ in figures 7 and 8, the areas under the curves are the pressure-drag coefficients of the flares provided a base pressure equal to free-stream pressure is assumed. The drag of the flare with the sharp lip is shown in figure 10. The results are not unexpected in the light of the schlieren and pressure results already shown. The presence of the flare bleed has had little effect on flare drag at Reynolds numbers of approximately 5×10^6 and 7×10^6. This is the result to be expected since the flow was attached in much the same manner regardless of the bleed size at these Reynolds numbers. At the lower Reynolds number of approximately 3.5×10^6, the data for no bleed and for a bleed-gap radial dimension of 0 are both about 30 percent below the values for the attached flow, but with

the larger bleeds, at the higher Reynolds numbers, the drag coefficients are in close agreement with the fully attached values. This result is again consistent with the appearance of the corresponding schlieren results. At the lowest Reynolds number $\left(R_L \approx 1.8 \times 10^6\right)$ the relative values of the data show the effect of the flare bleed gap in increasing the flare drag. These results agree with the observation that at these lowest Reynolds numbers the largest bleed gap used reduced the extent of the separation somewhat, but did not prevent separation. The faired pressure-drag curve from reference 7 has been added to figure 10 to show the trend found for a flare with no bleed over a slightly greater Reynolds number range.

L I 2 2 1

The drag of the flare with the blunt lip is shown in figure 11. The results shown here are similar in some respects to the results for the sharp-lip flare. Again the presence of the flare bleed had little effect upon the drag at the higher Reynolds numbers, since the flare bleed did not change the shape of the flow boundaries at Reynolds numbers of about 3.5×10^6 and above. At the two lowest test Reynolds numbers of about 1.9×10^6 and 1×10^6 the data show the extensive effect of the flare bleed gap upon the flare drag. With the largest bleeds the drag coefficients observed were in agreement with values for attached flow. This result was in accord with the schlieren observations which showed that separation was prevented even at the lowest Reynolds number by the largest two bleeds with the blunt flare. The size of the largest radial bleed gap for the blunt lip was more than double that of the largest radial bleed gap tested with a sharp lip, and again the conclusion is drawn that separation could have been prevented in the case of the sharp lip if a larger bleed had been tried.

Heat Transfer to Flare

The heat transfer to the flare with the sharp leading edge is shown in figure 12. The experimental results for this flare with no gap are similar to the findings of references 7 and 8. At the lowest test Reynolds number the separation is extensive, and reattachment occurs at the trailing edge of the flare. The heat transfer to the flare increases toward a maximum value near the trailing edge of the flare. At the next test Reynolds number, approximately twice the value of the lowest, the values of the heat transfer are higher and again they increase toward the reattachment point. The increased slope of this group of data may be attributed to the fact that transition of the separated boundary occurred over the flare surface. At the next highest Reynolds number the separated boundary was observed to reattach about midway between the start and the trailing edge of the flare. The heat transfer is observed to reach a maximum just behind the apparent

location of reattachment. These heat-transfer data are in fair agreement with the curve predicted by Van Driest's flat-plate turbulent theory (ref. 27) by using the Van Driest turbulent cone rule (ref. 28). In calculating this curve the boundary layer was assumed to start at the point of reattachment and the free-stream conditions were assumed to be those calculated behind the reattachment shock in the same manner as the pressures previously shown in figure 7. At the highest Reynolds number the extent of the separated region is very small and the heat transfer is a maximum near the start of the flare. In this case the data fall above the theory but with reasonable agreement.

To the right of the no-gap heat-transfer results in figure 12 are the results of tests with various-sized boundary-layer bleeds. The shape of the heat-transfer distribution is a direct result of the shape of the separated boundaries shown in figure 3 and the shape of the pressure distributions seen in figure 7. For the second set of data seen in figure 12, $x/D = 0.032$, and $y/D = 0$. The schlieren photographs show that this flare bleed gap had little effect upon shape of the separated region. Likewise, the heat-transfer results for this configuration show only a slight variation from the heat transfer of the configuration with no gap. In this instance a change in the dimension of the axial bleed gap had little effect on the aerodynamic and thermodynamic properties of the flow. As another example which shows the effect of a moderate change in the dimension of the axial bleed gap, consider the results for the models with a common radial bleed gap ($y/D = 0.032$) but with different axial bleed gaps ($x/D = 0$, and $x/D = 0.032$). Again the shapes of the separated boundaries as observed in the schlieren pictures for these two cases are little changed, and the heat-transfer results show only a slight variation. However, the data for these two configurations with the radial bleed gap are significantly different from the data for the two configurations with no radial bleed gap. The heat transfer to the flare in the separated region has been increased in the case of the larger gap, but the most significant change has been the reduction in the heat transfer with fully attached flow. This heat-transfer reduction, as well as its agreement with the shape of the laminar-theory curve (ref. 27) corrected for three-dimensional effects by the Mangler transformation (ref. 29), suggests that the turbulent boundary layer has been removed and a laminar boundary layer has been started on the surface of the flare. These decreased heat-transfer data do not agree with the level of the laminar theory, however, but tend to fall about halfway between the laminar-theory curve and the turbulent-theory curve. At $R_L \approx 3.5 \times 10^6$ it appears from the shape of the curve that the boundary layer remains laminar over the entire surface of the flare, while at $R_L \approx 7 \times 10^6$ the start of transition on the flare is indicated by the trend of the data. The data in figure 12(e) are for the same radial bleed gap ($y/D = 0.032$) as

L
1
2
2
1

figures 12(c) and 12(d), but for a much larger axial bleed gap ($x/D = 0.172$). The heat-transfer results in this case are shown to be increased above those shown in the previous two cases for the highest Reynolds number ($R_L \approx 6.8 \times 10^6$) and for the lowest Reynolds number ($R_L \approx 1.1 \times 10^6$), but the heat-transfer results for the intermediate Reynolds number ($R_L \approx 3.6 \times 10^6$) show little change.

The results of using flare bleed gaps when the leading edge is blunt are shown in figure 13. The data for the configuration with no bleed are again shown for comparison. It is apparent that the gap with the blunt lip is not as effective as the gap with the sharp lip in reducing the heat transfer at Reynolds numbers high enough to cause attached flow without a bleed. This difference in effectiveness must be caused at least partly by the thickening and by a possible slight separation of the boundary layer which has been mentioned before in connection with the blunt-lip schlieren data and which can reduce the stability of the boundary layer. At lower Reynolds numbers, where reattachment occurs on the surface of the flare in back of the leading edge, the heat-transfer results for the blunt lip appear to be more similar to the sharp-lip results.

L-1221

Possible heat transfer to the inside of the flare has not been taken into account for any of the flare heat-transfer calculations. The pressures and flow velocities inside the flare were expected to be low and to contribute little to the heat transfer to the flare. Nevertheless, the magnitude of the internal heat transfer to the flare is uncertain, and it can be expected to increase with an increase in the internal flare pressure. In the cases previously mentioned where the heat-transfer data fell above the corresponding theory, the discrepancy between data and theory can possibly be explained by heat transfer to the inside skin of the flare. Furthermore, in the heat-transfer tests at the highest Reynolds number with very large bleed gaps shown in figures 12(e), 13(h), 13(i), and 13(j), the pressure inside the flare was approximately double the free-stream pressure. This increased pressure was probably due to flow blockage at the exit orifices of the flare. These heat-transfer results are especially subject to question. It must be remembered, however, that any appreciable heat transfer to the inside of the flare strengthens the conclusion that heat transfer to the outside of the flare is reduced by the flare bleed gap, since it is reasonable to expect the heat transfer to the inside of the flare to increase with an increase in the mass flow through the flare bleed gap.

The Effectiveness of the Flares

The previous discussion has shown that both pressure and heat transfer on the surface of the flare are greatly affected by the extent

of separation, the Reynolds number, and the shape and size of the flare bleed. The effectiveness of the flare in producing drag with a minimum of heat transfer may be studied by observing the ratio $C_{Dp}/\bar{N}_{St}$. For maximum effectiveness of the flare, the value of $C_{Dp}/\bar{N}_{St}$ should be a maximum.

The effect of Reynolds number upon the ratio $C_{Dp}/\bar{N}_{St}$ has previously been studied for a similar body shape with no gap in reference 7. Even though the heat transfer was increased by an increase in Reynolds number in that investigation the increase in drag as a direct result of the decrease in separation was greater than the increase in heat transfer. Thus it was shown that the ratio $C_{Dp}/\bar{N}_{St}$ was increased by an increase in Reynolds number in the range of the conditions of the tests. Therefore it was considered likely that the ability to reduce the heat transfer at high Reynolds numbers by bleeding off the turbulent boundary layer, or the ability to increase the pressure drag at lower Reynolds numbers by preventing the separation, could lead to an even greater increase in the ratio $C_{Dp}/\bar{N}_{St}$ over a greater range of Reynolds numbers. L 1 2 2. 1

The results in figure 14 verify this idea. The highest values of $C_{Dp}/\bar{N}_{St}$ were realized with the sharp-lip flare, and were 50 percent above the highest values observed for this same flare with no gap. High values of $C_{Dp}/\bar{N}_{St}$ were realized at Reynolds numbers of about 3.5×10^6, where the sharp-lip flare with a radial gap showed values more than double the maximum value of the same flare with no gap. At lower Reynolds numbers of about 1.9×10^6 the sharp-lip flare was unable to prevent separation and $C_{Dp}/\bar{N}_{St}$ dropped to a low value. The blunt leading edge prevented an increase in $C_{Dp}/\bar{N}_{St}$ over the no-gap results at the highest Reynolds numbers since it interfered with the start of a laminar boundary layer on the surface of the flare, but the blunt lip with the largest bleed gap allowed favorably high values of $C_{Dp}/\bar{N}_{St}$ over a Reynolds number range extended to as low as 1×10^6. This was the configuration which prevented separation at all test Reynolds numbers (see fig. 4(h)). If a wider gap were used with the sharp-lip flare, it may be surmised that the even higher values of $C_{Dp}/\bar{N}_{St}$ characteristic of this configuration would be extended to the same low Reynolds number.

CONCLUSIONS

These tests of an ogive-cylinder body followed by a 30° half-angle flare at a Mach number of approximately 6.8 and Reynolds numbers from 1×10^6 to 7.4×10^6, based on free-stream conditions and the forebody length, have led to the following conclusions:

1. An adequate boundary-layer bleed at the start of a flare may be used to prevent or reduce the extensive separation characteristic of the laminar boundary layer, or it may be used to remove the turbulent boundary layer ahead of the flare and allow the start of a laminar boundary layer on the surface of the flare with a reduction in heat transfer.

2. Blunting the leading edge of the flare, as may be necessary to preserve it from high-temperature destruction, appears to interfere with its effectiveness in removing a turbulent boundary layer ahead of the flare and in allowing the start of a new laminar boundary layer at the start of the flare.

3. The use of a flare bleed can increase the value of $C_{Dp}/\bar{N}_{St}$ and allow the realization of high values of $C_{Dp}/\bar{N}_{St}$ over an extended Reynolds number range, and therefore can increase the effectiveness of the use of a flare as a drag brake.

4. Under the conditions of these tests the radial dimension of the bleed was of prime importance, the axial dimension being of lesser importance.

5. The pressures on the surface of the flare may be approximated from the angles between the separated boundary layer and the flare wall at reattachment by assuming two-dimensional wedge flow at the start of separation and at reattachment.

6. The heat transfer to the flare in the region behind reattachment may be approximated by assuming the boundary layer to start at the point of reattachment and by using the proper local stream conditions and a suitable flat-plate theory.

Langley Research Center,
National Aeronautics and Space Administration,
Langley Field, Va., October 11, 1960.

REFERENCES

1. Chapman, Dean R., Kuehn, Donald M., and Larson, Howard K.: Investigation of Separated Flows in Supersonic and Subsonic Streams With Emphasis on the Effect of Transition. NACA Rep. 1356, 1958. (Supersedes NACA TN 3869.)

2. Gadd, G. E., Holder, D. W., and Regan, J. D.: An Experimental Investigation of the Interaction Between Shock Waves and Boundary Layers. Proc. Roy. Soc. (London), ser. A, vol. 226, no. 1165, Nov. 9, 1954, pp. 227-253.

3. Chuan, Raymond L.: An Investigation of Shock Wave-Boundary Layer Interaction. USCEC Rep. 40-101 (AFOSR TR-58-145, AD 302 753), Univ. of Southern California, Aug. 1958.

4. Bernstein, Harry, and Brunk, William E.: Exploratory Investigation of Flow in the Separated Region Ahead of Two Blunt Bodies at Mach Number 2. NACA RM E55D07b, 1955.

5. Kuehn, Donald M.: Experimental Investigation of the Pressure Rise Required for the Incipient Separation of Turbulent Boundary Layers in Two-Dimensional Supersonic Flow. NASA MEMO 1-21-59A, 1959.

6. Crawford, Davis H.: Investigation of the Flow Over a Spiked-Nose Hemisphere-Cylinder at a Mach Number of 6.8. NASA TN D-118, 1959.

7. Becker, John V., and Korycinski, Peter F.: Heat Transfer and Pressure Distribution at a Mach Number of 6.8 on Bodies With Conical Flares and Extensive Flow Separation. NACA RM L56F22, 1956.

8. Crawford, Davis H., and Rumsey, Charles B.: Heat Transfer in Regions of Separated and Reattached Flows. NACA RM L57D25b, 1957.

9. Reese, David E., Jr., and Wehrend, William R., Jr.: An Investigation of the Static and Dynamic Aerodynamic Characteristics of a Series of Blunt-Nosed Cylinder-Flare Models at Mach Numbers From 0.65 to 2.20. NASA TM X-110, 1960.

10. Wakefield, Roy M., Knechtel, Earl D., and Treon, Stuart L.: Transonic Static Aerodynamic Characteristics of a Blunt Cone-Cylinder Body With Flared Afterbodies of Various Angles and Base Areas. NASA TM X-106, 1959.

11. Dennis, David H.: The Effects of Boundary-Layer Separation Over Bodies of Revolution With Conical Tail Flares. NACA RM A57I30, 1957.

12. Dennis, David H., and Syvertson, Clarence A.: Effects of Boundary-Layer Separation on Normal Force and Center of Pressure of a Cone-Cylinder Model With a Large Base Flare at Mach Numbers From 3.00 to 6.28. NACA RM A55H09, 1955.

13. Hall, James R., and Graham, John B., Jr.: Aerodynamic Heating and Lateral Force Measurements of a Blunt-Nose Flare-Cylinder Configuration Undergoing Large Lateral Oscillations at Mach Numbers up to 10.15. NASA TM X-45, 1959.

14. Baber, Hal T., Jr., and Henning, Allen B.: Stability Characteristics From Mach Number 1.0 to 3.2 of a Missile of Fineness Ratio 11.5 With a 10° Flared-Skirt Afterbody. NASA MEMO 4-2-59L, 1959.

15. Chapman, Dean R.: A Theoretical Analysis of Heat Transfer in Regions of Separated Flow. NACA TN 3792, 1956.

16. Burrows, F. M., and Newman, B. G.: The Application of Suction to a Two-Dimensional Laminar Separation Bubble. Res. Rep. # 27 (Contract Nonr 978(01), The Aerophys. Dept., Mississippi State Univ., Oct. 1, 1959.

17. McLellan, Charles H., Williams, Thomas W., and Bertram, Mitchel H.: Investigation of a Two-Step Nozzle in the Langley 11-Inch Hypersonic Tunnel. NACA TN 2171, 1950.

18. McLellan, Charles H., Williams, Thomas W., and Beckwith, Ivan E.: Investigation of the Flow Through a Single-Stage Two-Dimensional Nozzle in the Langley 11-Inch Hypersonic Tunnel. NACA TN 2223, 1950.

19. Stollery, J. L., Maull, D. J., and Belcher, B. J.: The Imperial College Hypersonic Gun Tunnel; August 1958-July 1959. Jour. R.A.S., vol. 64, no. 589, Jan. 1960.

20. Mair, W. A.: Experiments on Separation of Boundary Layers on Probes in Front of Blunt-Nosed Bodies in a Supersonic Air Stream. Phil. Mag., ser. 7, vol. 43, no. 342, July 1952, pp. 695-716.

21. Bogdonoff, Seymour M., and Vas, Irwin E.: Preliminary Investigations of Spiked Bodies at Hypersonic Speeds. Jour. Aero. Sci., vol. 26, no. 2, Feb. 1959, pp. 65-74.

22. Love, Eugene S.: Base Pressure at Supersonic Speeds on Two-Dimensional Airfoils and on Bodies of Revolution With and Without Fins Having Turbulent Boundary Layers. NACA TN 3819, 1957. (Supersedes NACA RM L53C02.)

23. Reller, John O., Jr., and Hamaker, Frank M.: An Experimental Investigation of the Base Pressure Characteristics of Nonlifting Bodies of Revolution at Mach Numbers From 2.73 to 4.98. NACA TN 3393, 1955. (Supersedes NACA RM A52E20.)

24. Hastings, R. C.: A Note on the Interpretation of Base Pressure Measurements in Supersonic Flows. C.P. No. 409, British A.R.C., 1958.

25. Reid, J.: The Estimation of Afterbody and Base Pressures in Axi-Symmetric Supersonic Flow at High Reynolds Numbers. Tech. Note No. Aero 2420, British R.A.E., Nov. 1955.

26. Bertram, Mitchel H., and Feller, William V.: A Simple Method for Determining Heat Transfer, Skin Friction, and Boundary-Layer Thickness for Hypersonic Laminar Boundary-Layer Flows in a Pressure Gradient. NASA MEMO 5-24-59L, 1959.

27. Van Driest, E. R.: The Problem of Aerodynamic Heating. Aero. Eng. Rev., vol. 15, no. 10, Oct. 1956, pp. 26-41.

28. Van Driest, E. R.: Turbulent Boundary Layer on a Cone in a Supersonic Flow at Zero Angle of Attack. Jour. Aero. Sci., vol. 19, no. 1, Jan. 1952, pp. 55-57, 72.

29. Mangler, W.: Compressible Boundary Layers on Bodies of Revolution. Reps. and Translations No. 47, British M.A.P. Völkenrode, Mar. 15, 1946.

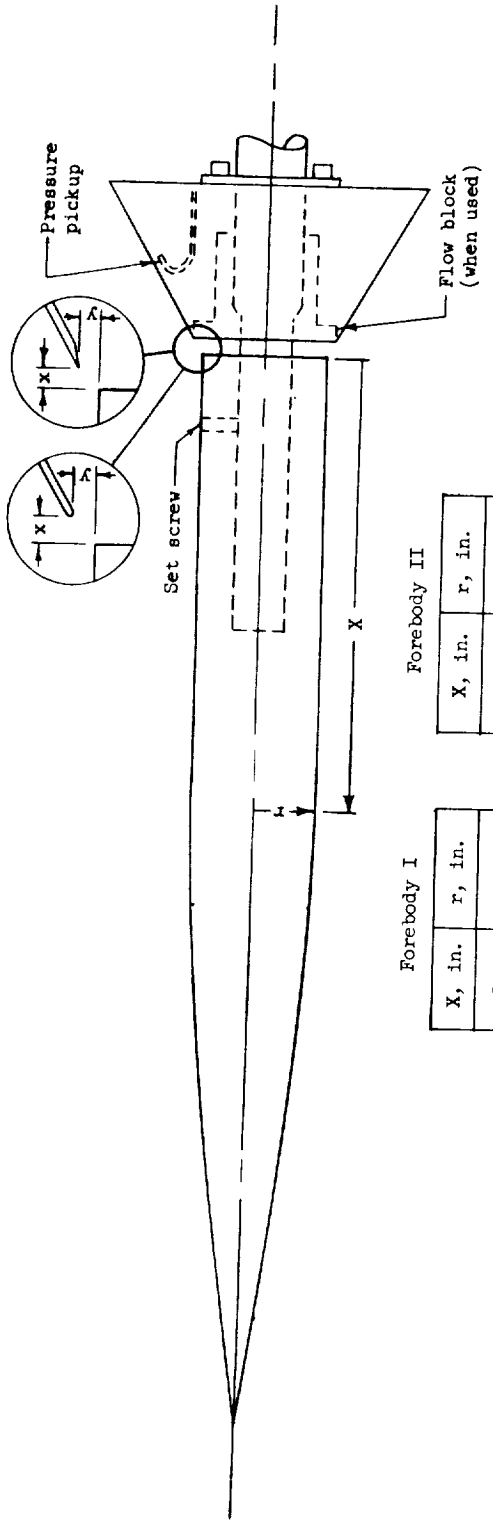

Forebody I

X, in.	r, in.
0	0.750
7.75	.750
8.25	.739
8.75	.720
9.25	.695
9.75	.665
10.25	.631
[illegible]	[illegible]
11.25	.553
11.75	.508
12.25	.459
12.75	.405
13.25	.347
13.75	.283
14.25	.211
14.50	.171
14.625	.150 } *
15.474	0 } *

Forebody II

X, in.	r, in.
0	0.900
6.205	.900
6.805	.887
7.405	.863
8.005	.834
8.578	.798
9.205	.757
[illegible]	[illegible]
9.865	.663
11.005	.609
11.605	.550
12.205	.486
12.805	.417
13.405	.340
14.005	.253
14.305	.205
14.455	.180 } *
15.474	0 } *

*Model conical in this region.

Figure 1.- Details of assembled model.

L-1221

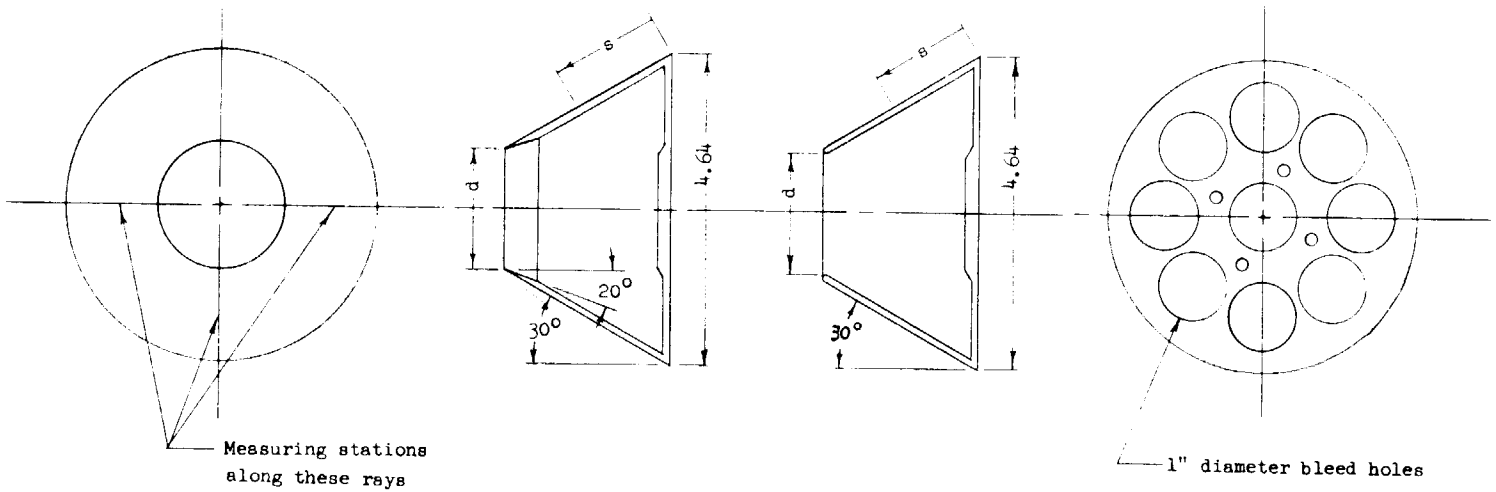

THERMOCOUPLE LOCATIONS

Distance to thermocouple, S, in., for -		
Sharp flare; d = 1.80 in.	Blunt flare; d = 1.80 in.	Blunt flare; d = 2.10 in.
0.31	0.31	0.31
.56	.56	.56
.81	.81	.81
1.06	1.06	1.06
1.31	1.31	1.31
1.56	1.56	1.56
1.81	1.81	1.81
2.06	2.06	2.06
2.31	2.31	
	2.56	
S = 2.84 in.	S = 2.64 in.	S = 2.34 in.

PRESSURE-ORIFICE LOCATIONS

Distance to pressure orifice, S, in., for -		
Sharp flare; d = 1.80 in.	Blunt flare; d = 1.80 in.	Blunt flare; d = 2.10 in.
0.56	0.56	0.31
2.31	2.31	.81
		1.19
		1.56
		2.06

Figure 2.- Details of model flares. All dimensions are in inches unless otherwise indicated.

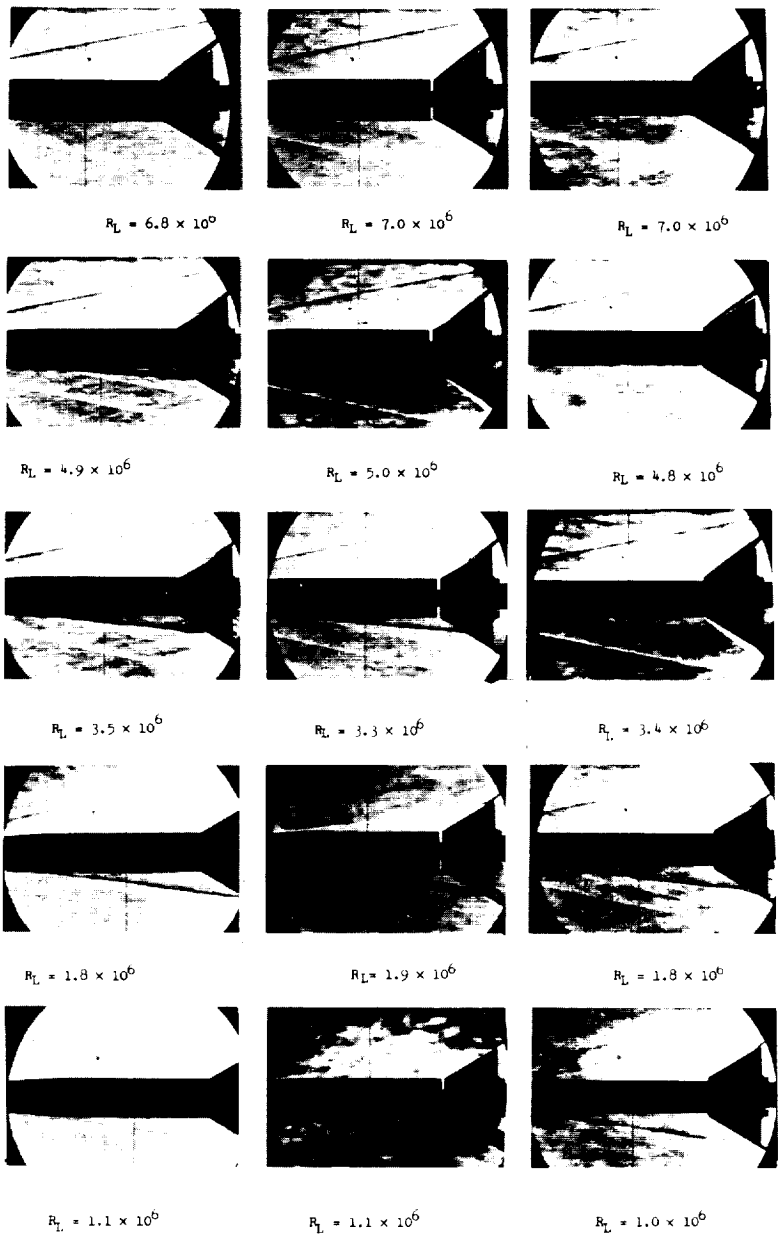

(a) x/D = 0; y/D = 0.

(b) x/D = 0.032; y/D = 0.

(c) x/D = 0; y/D = 0.032.

L-60-6942

Figure 3.- Schlieren photographs of flow over models with sharp-leading-edge flare.

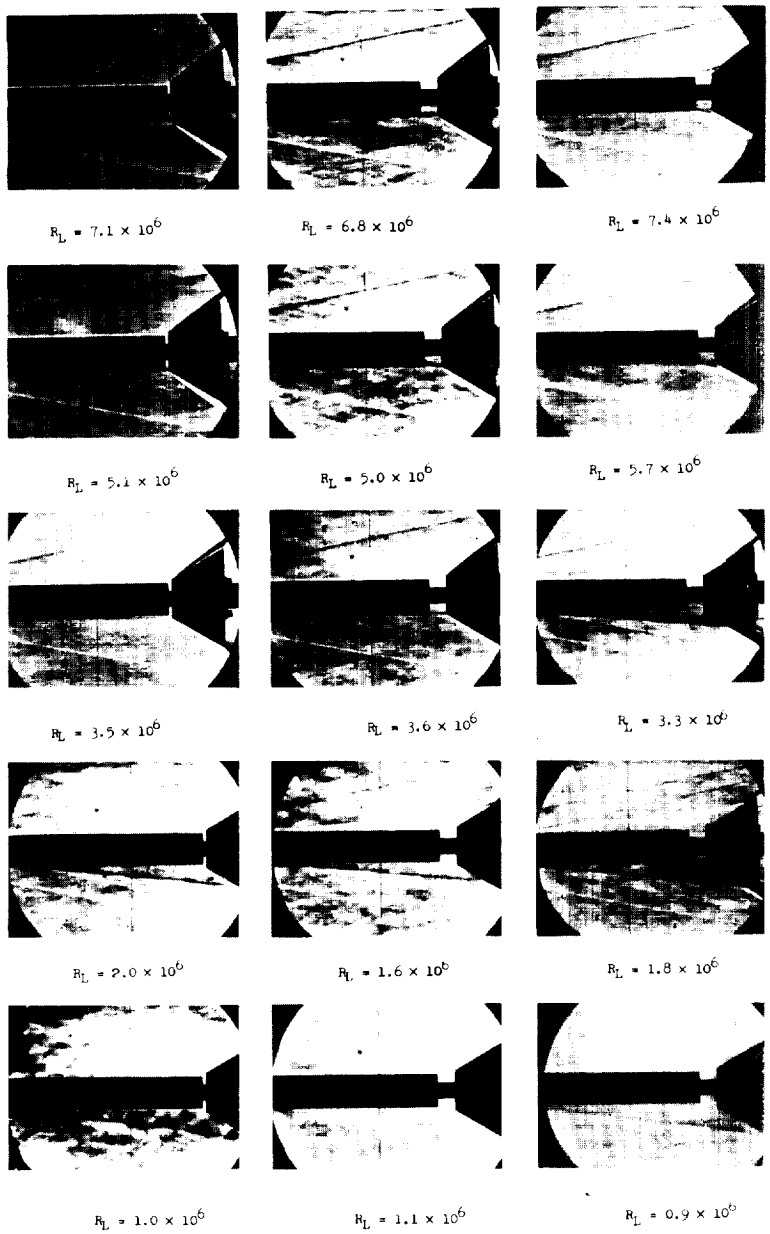

(d) x/D = 0.032; y/D = 0.032.

(e) x/D = 0.172; y/D = 0.032.

(f) x/D = 0.172; y/D = 0.032. (flow blocked in flare).

Figure 3.- Concluded. L-60-6943

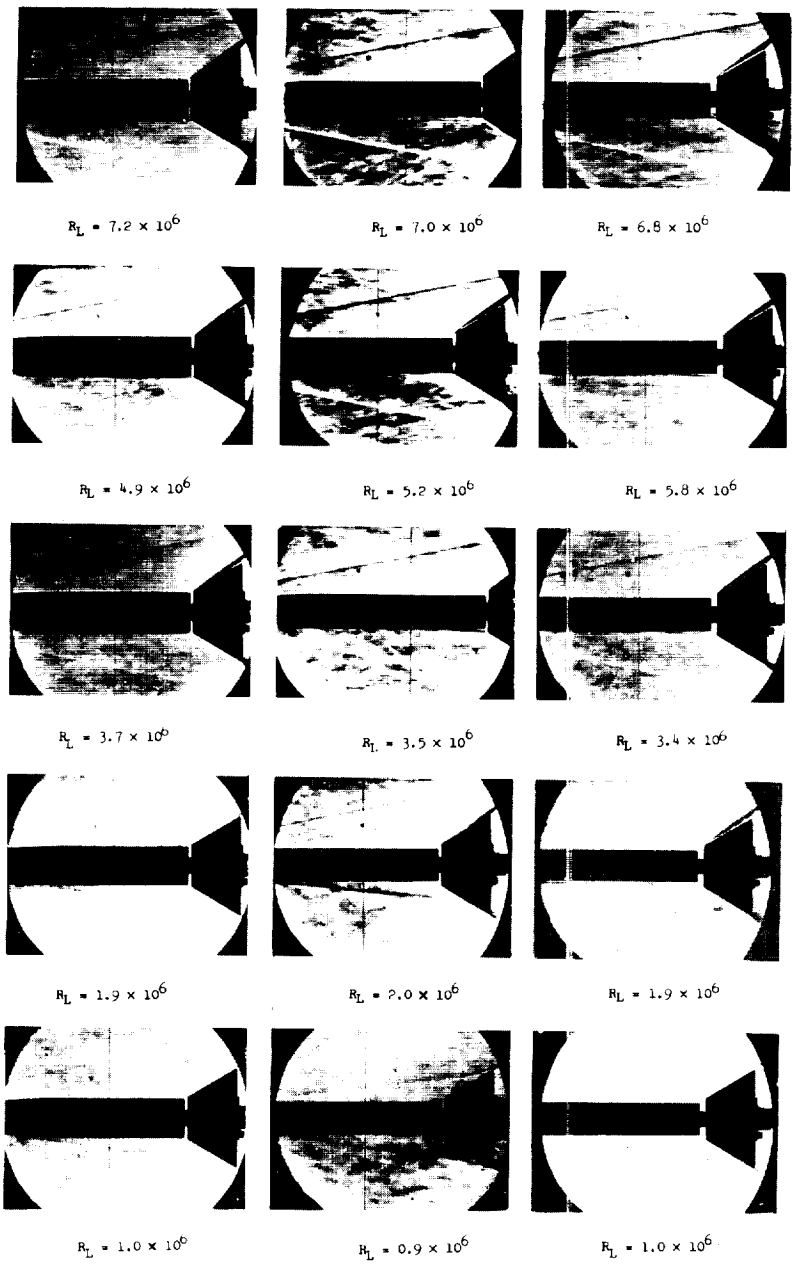

(a) x/D = 0.030; y/D = 0.

(b) x/D = 0.030; y/D = 0.032.

(c) x/D = 0.062; y/D = 0.032.

L-60-6944

Figure 4.- Schlieren photographs of flow over models with blunt-leading-edge flare.

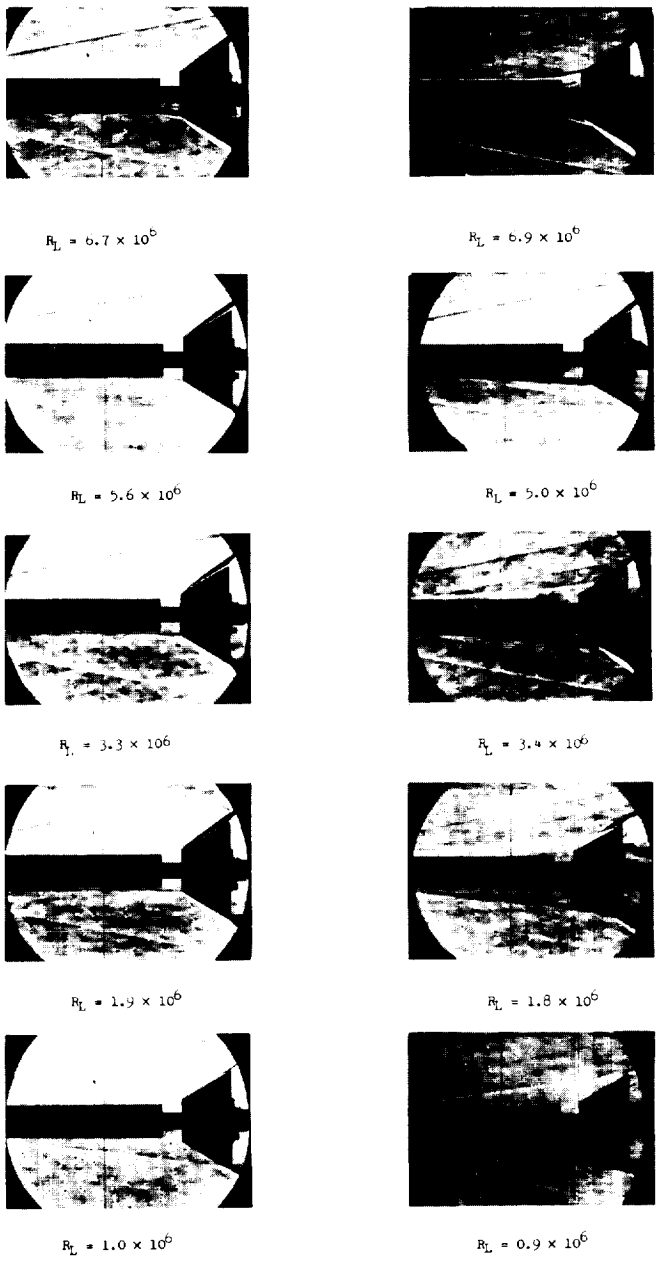

(d) x/D = 0.202; y/D = 0.032.

(e) x/D = 0.202; y/D = 0.032 (flow blocked in flare).

Figure 4.- Continued. L-60-6945

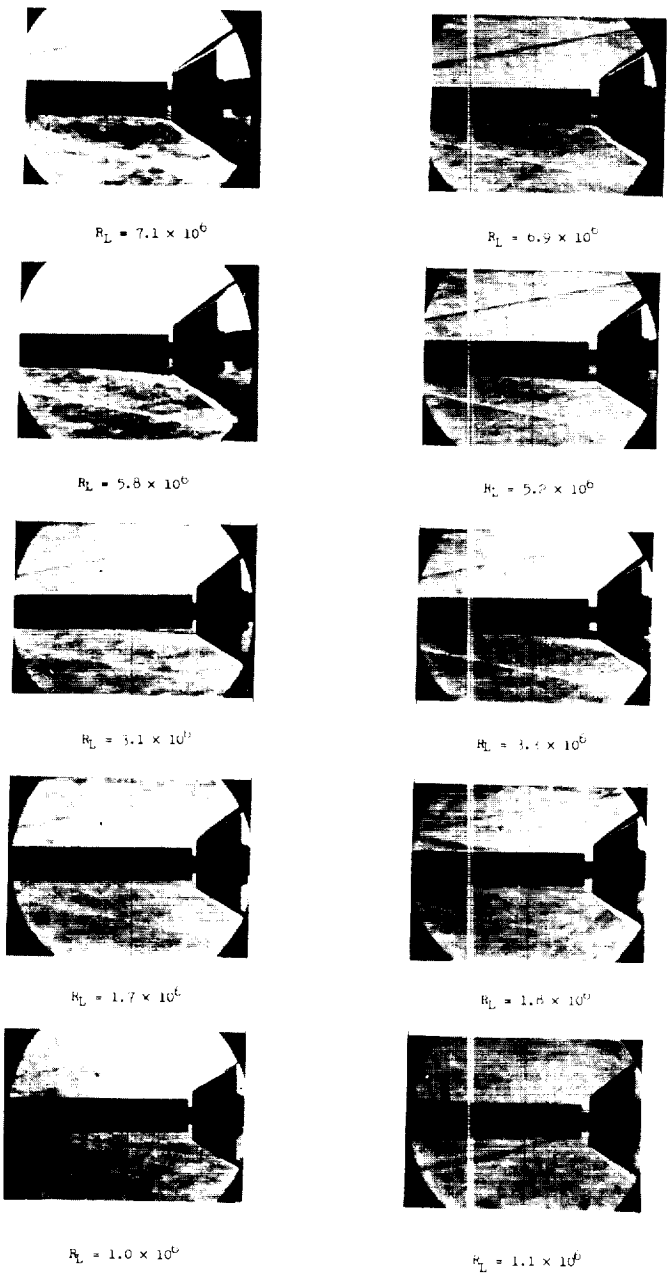

(f) x/D = 0.048; y/D = 0.065. (g) x/D = 0.094; y/D = 0.065.

Figure 4.- Continued. L-60-6946

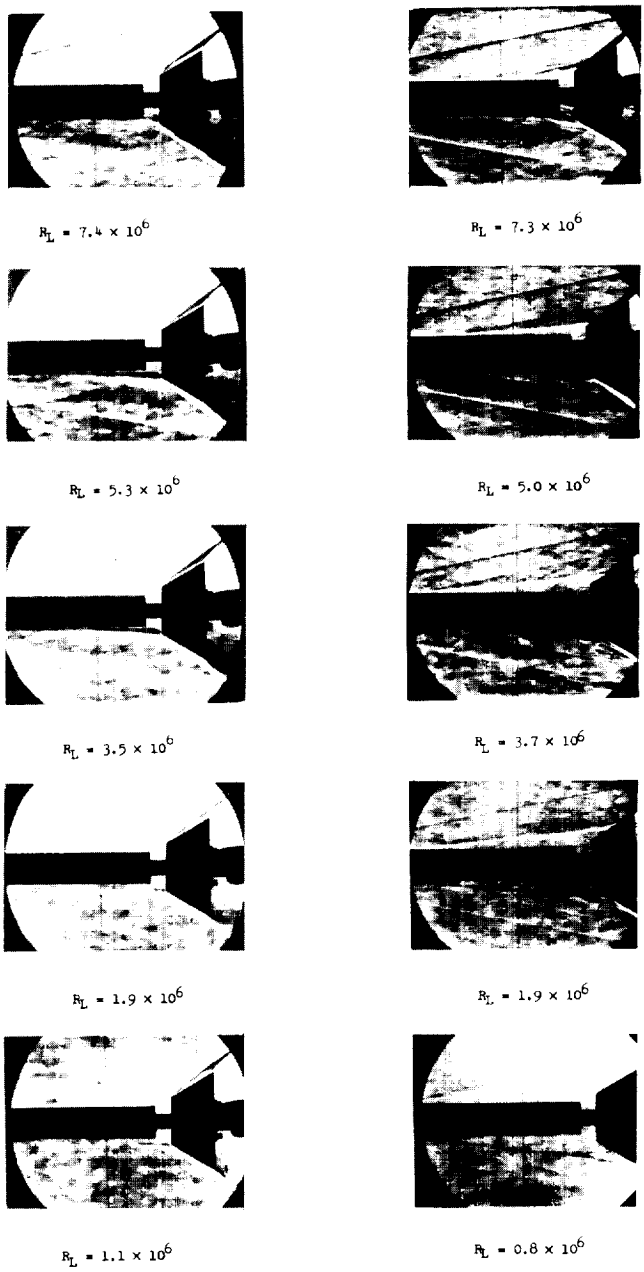

(h) x/D = 0.159; y/D = 0.065. (i) x/D = 0.159; y/D = 0.065 (flow blocked in flare).

Figure 4.- Concluded. L-60-6947

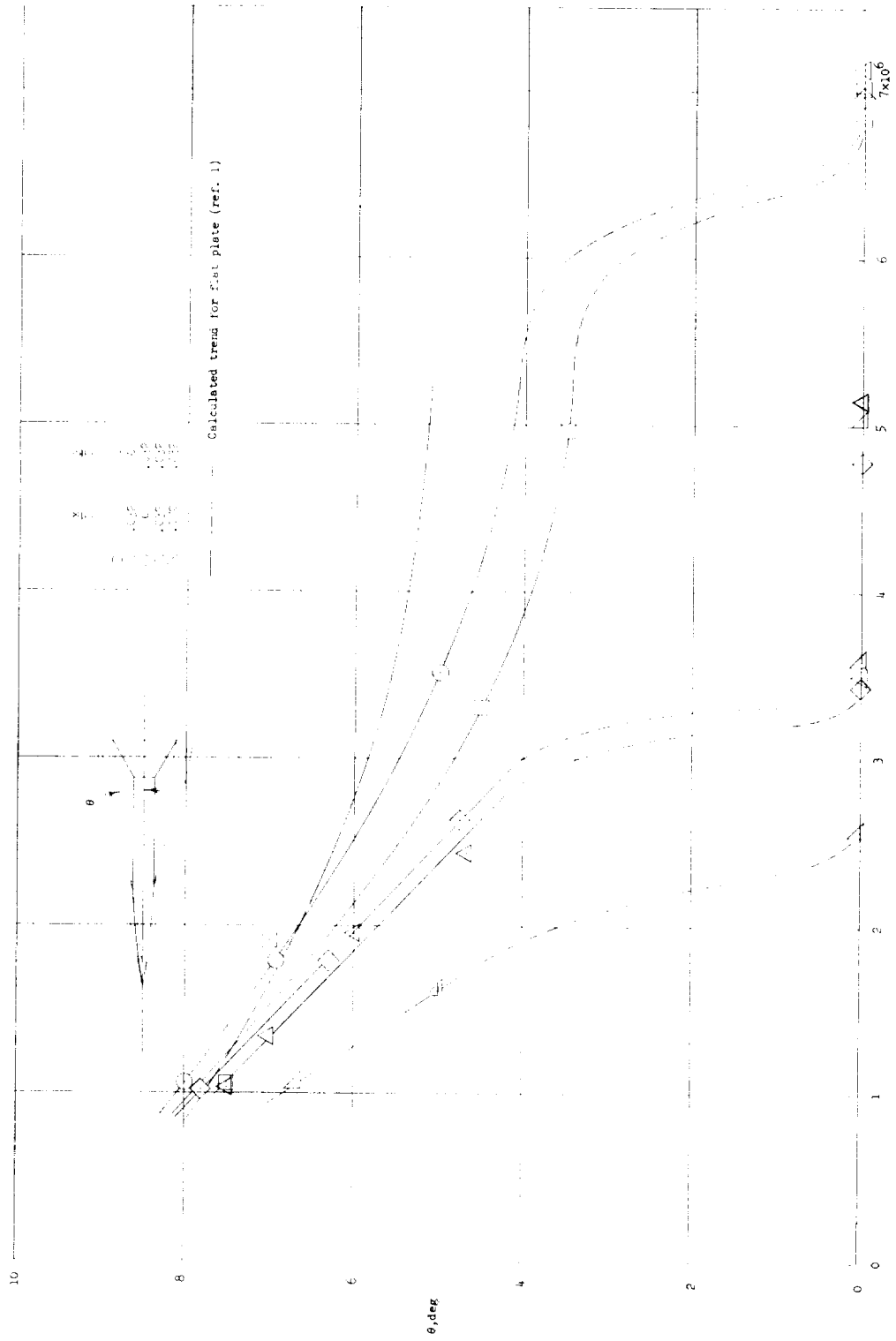

Figure 5.- Effect of bleed dimensions and Reynolds number on angle of separation for sharp-leading-edge flare.

L-1221

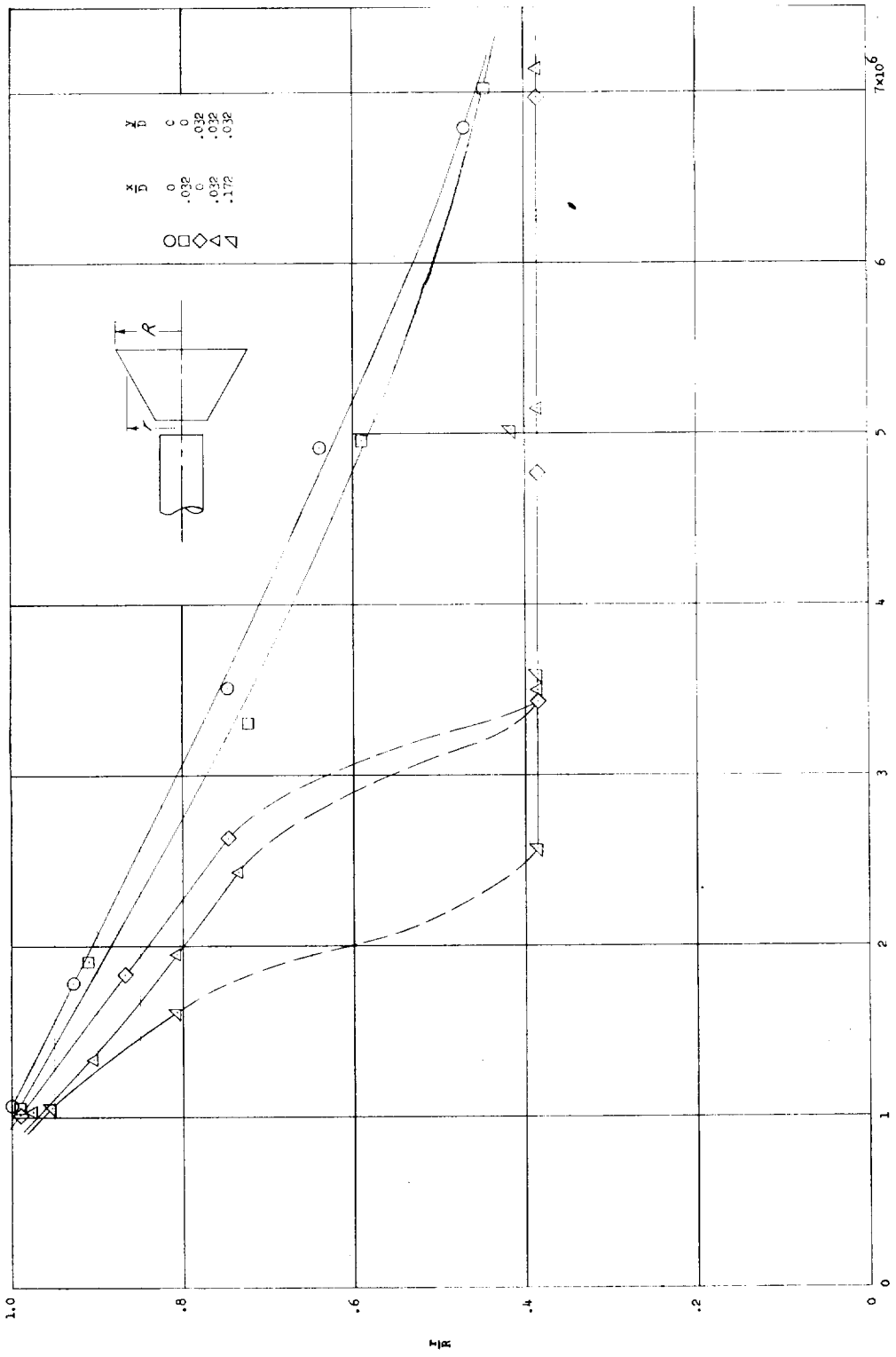

Figure 6.- Location of reattachment to sharp-leading-edge flare.

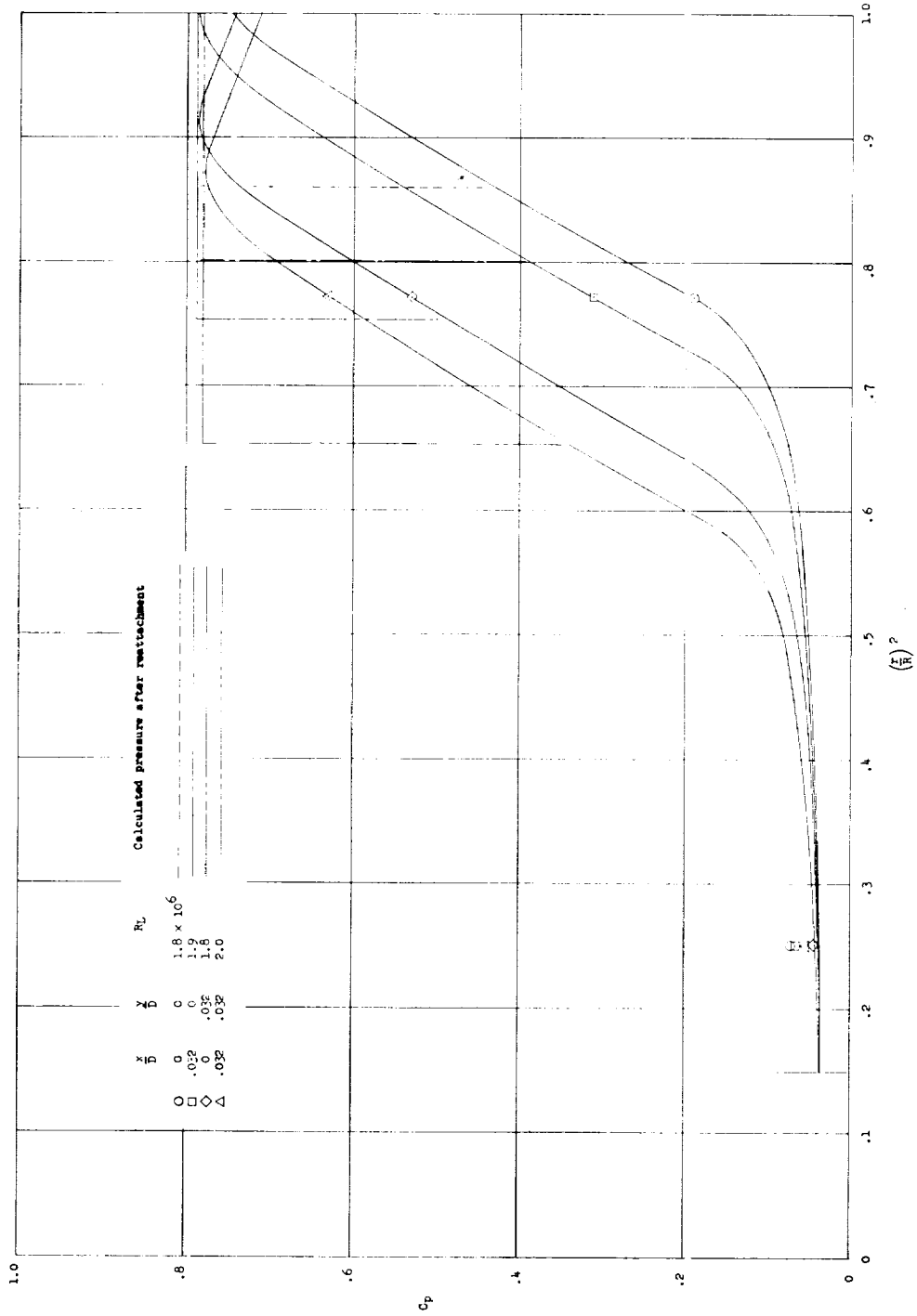

(a) $R_L \approx 1.9 \times 10^6$.

Figure 7.- Experimental and computed pressures on sharp-leading-edge flare.

L-1221

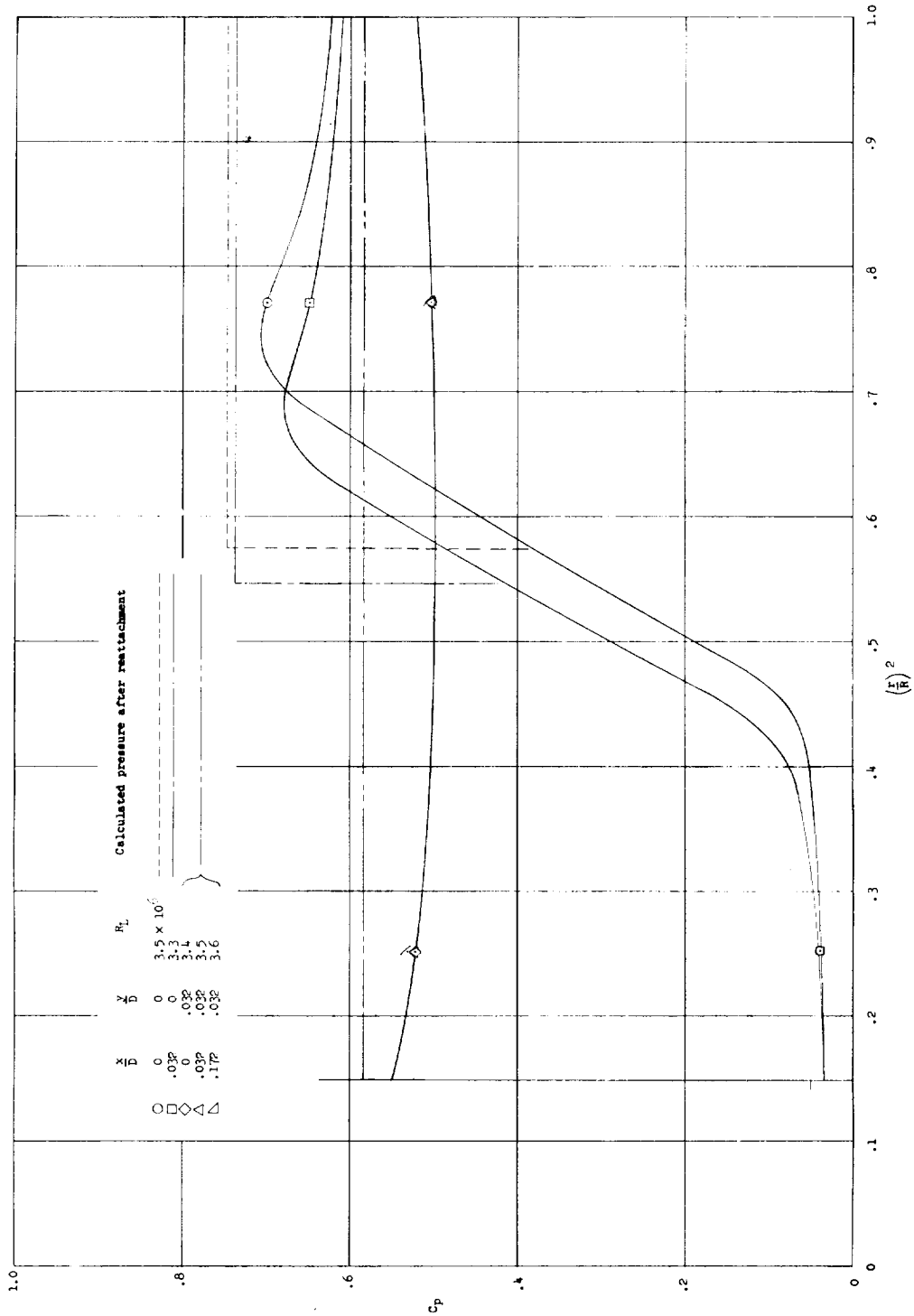

(b) $R_L \approx 3.5 \times 10^6$.

Figure 7.- Continued.

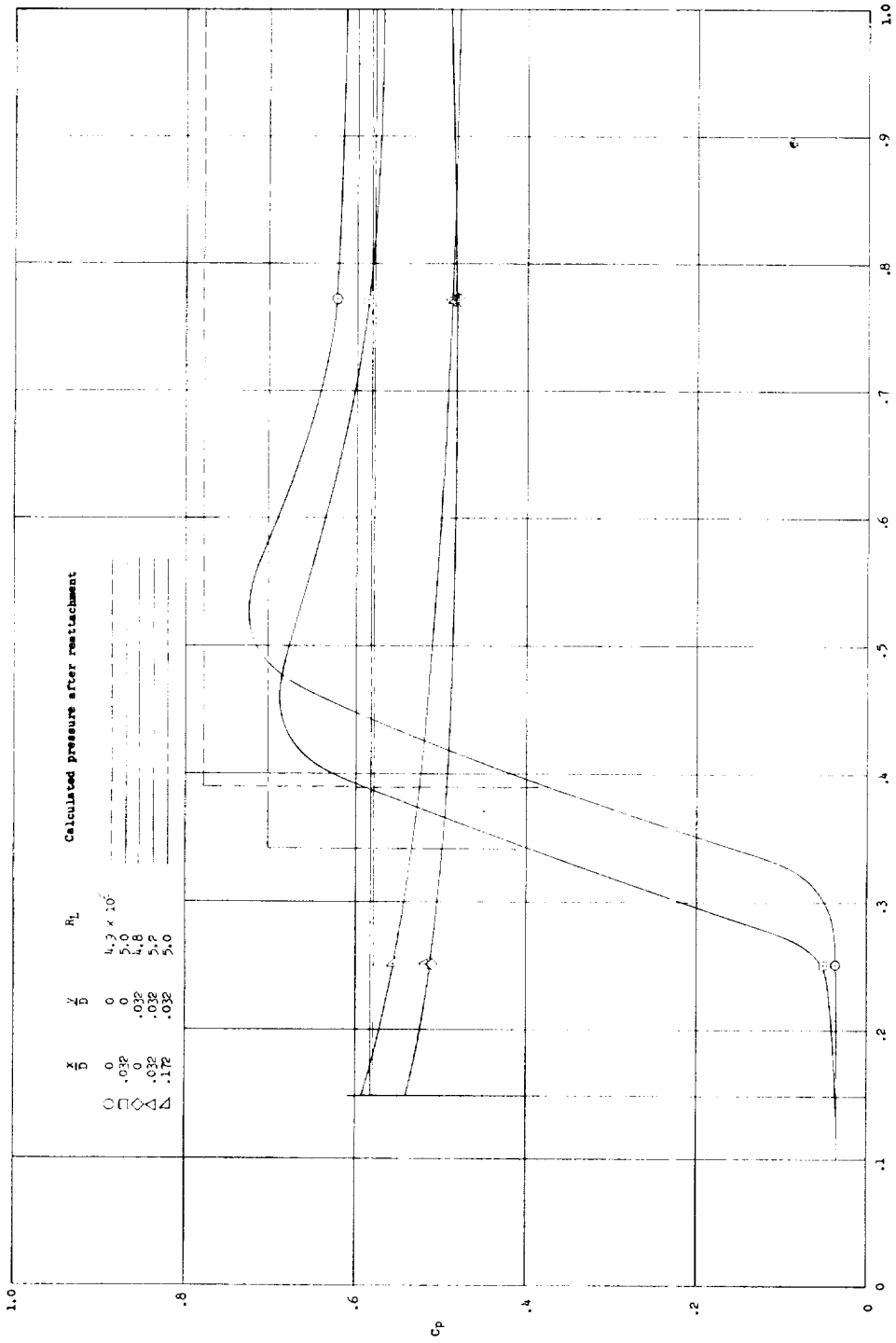

(c) $R_L \approx 5.0 \times 10^6$.

Figure 7.- Continued.

L-1221

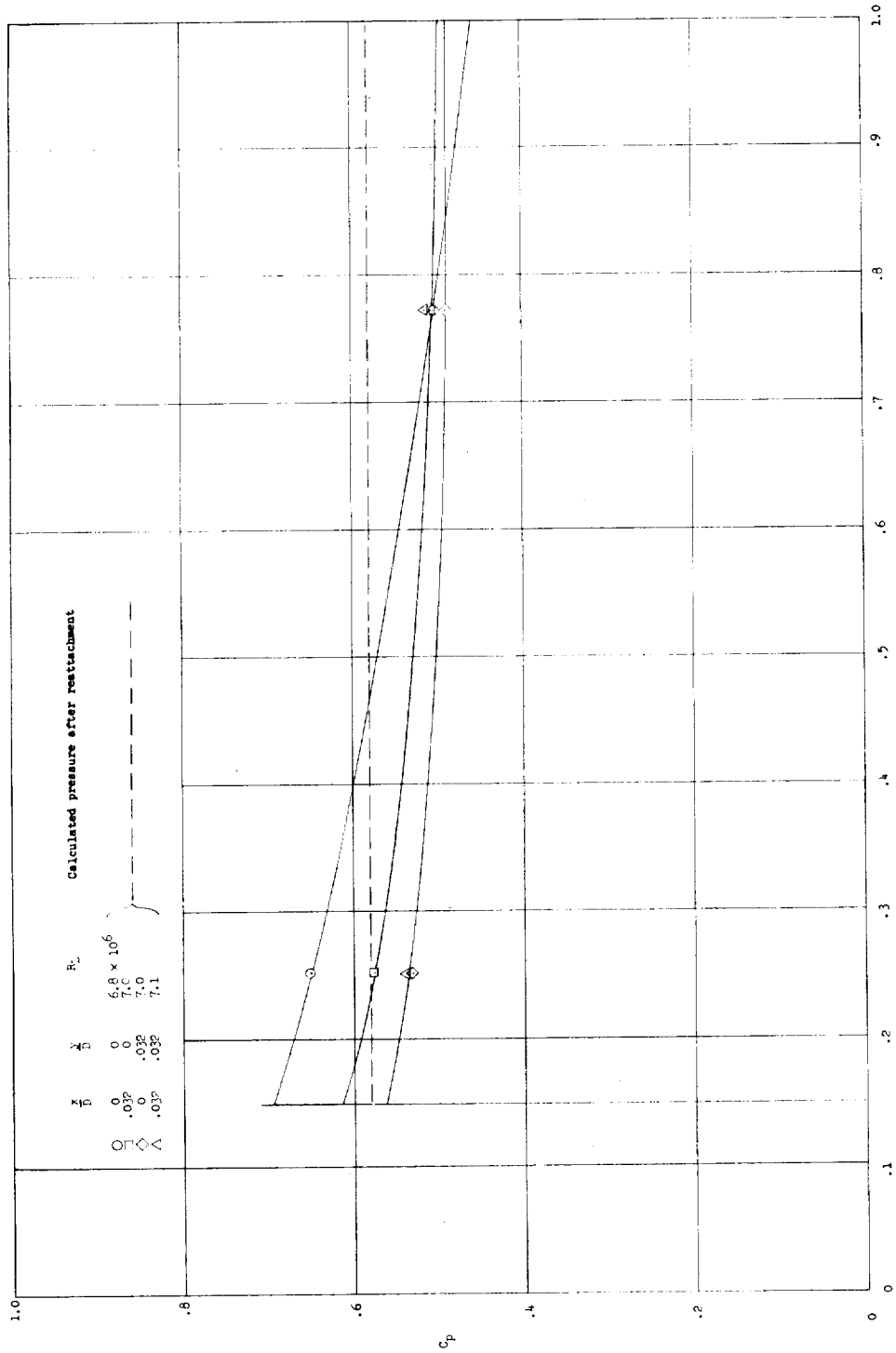

(d) $R_L \approx 7.0 \times 10^6$.

Figure 7.- Concluded.

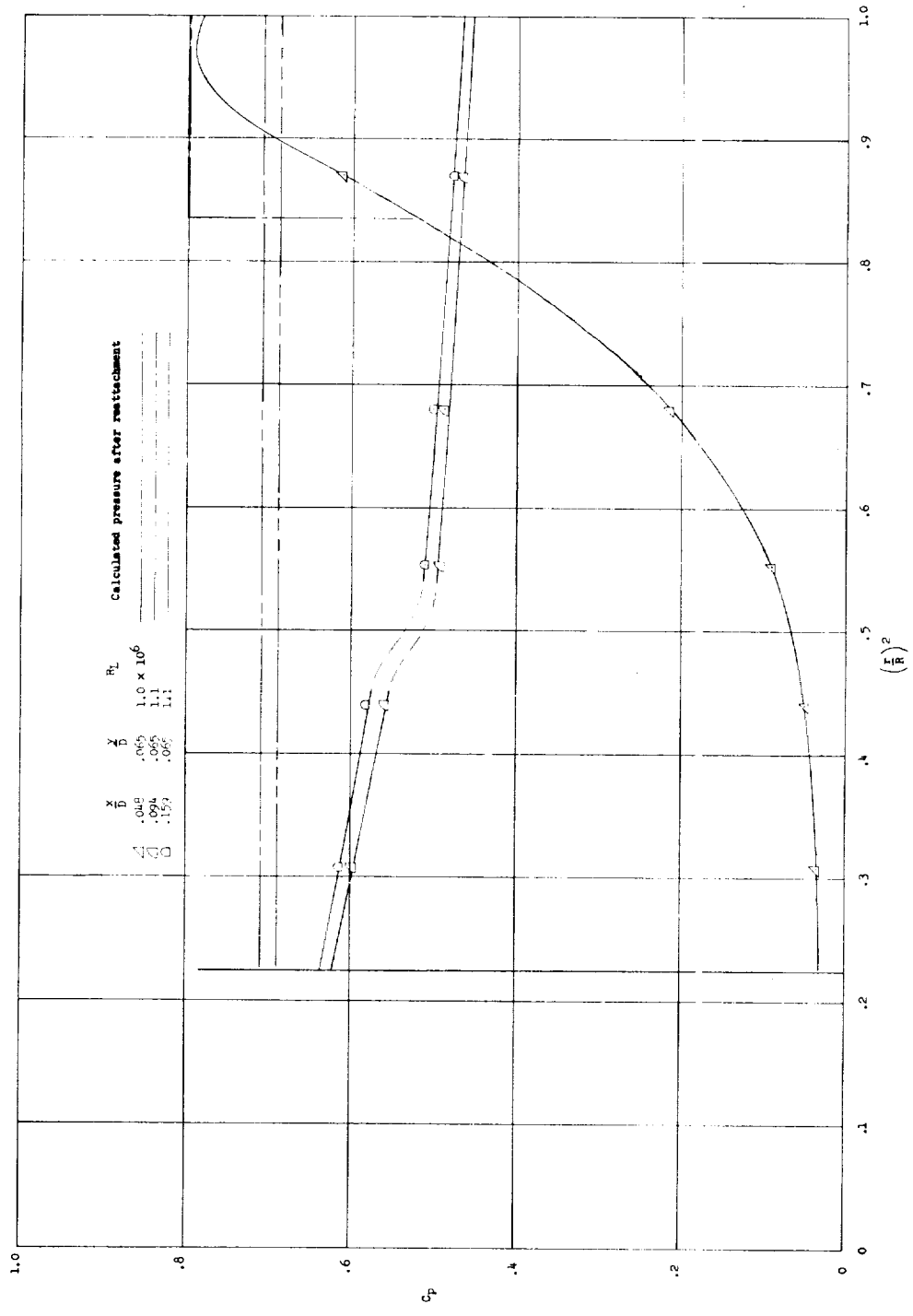

(a) $R_L \approx 1.1 \times 10^6$.

Figure 8.- Experimental and computed pressures on blunt-leading-edge flare.

L-1221

L-1221

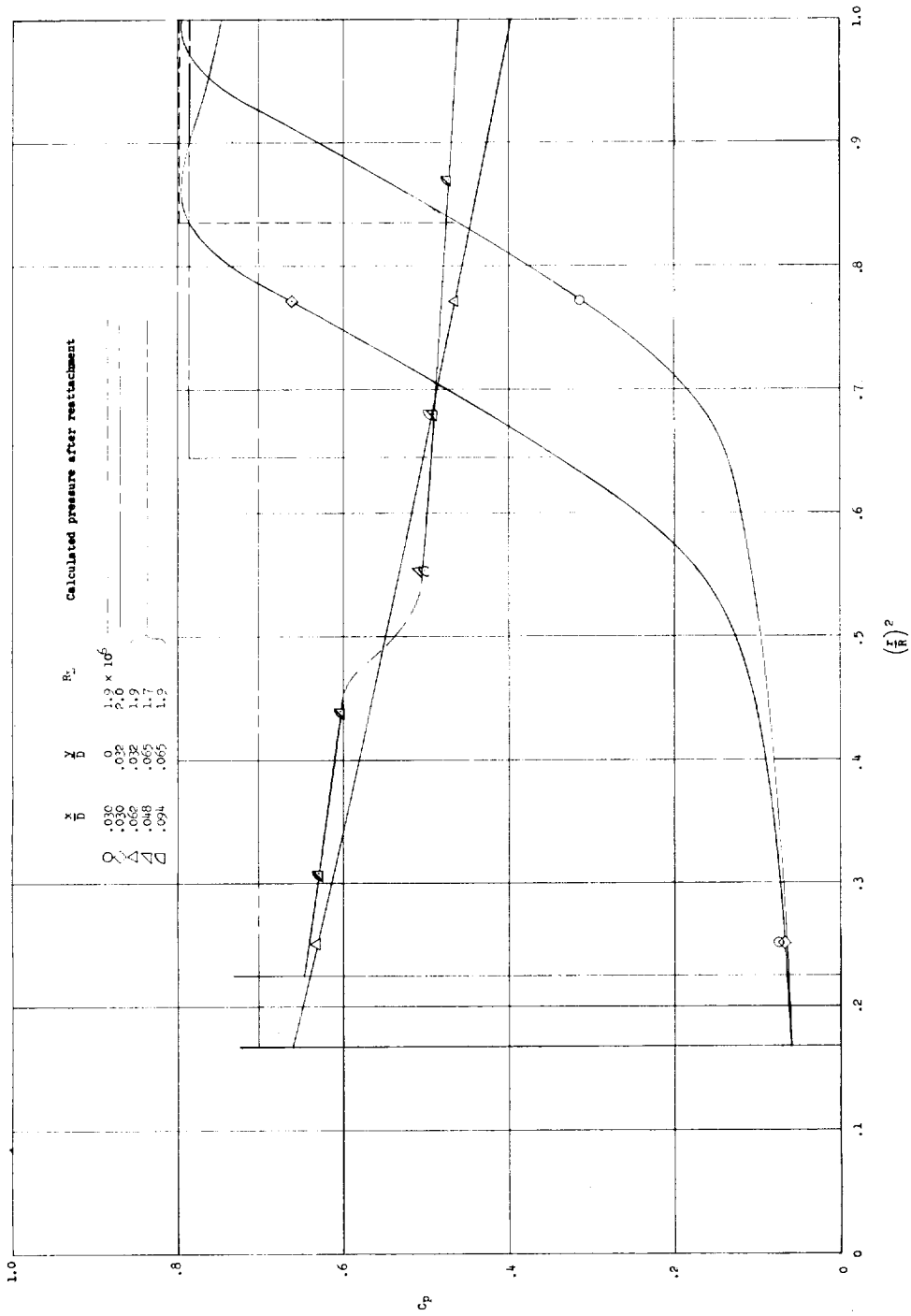

(b) $R_L \approx 1.9 \times 10^6$.

Figure 8.- Continued.

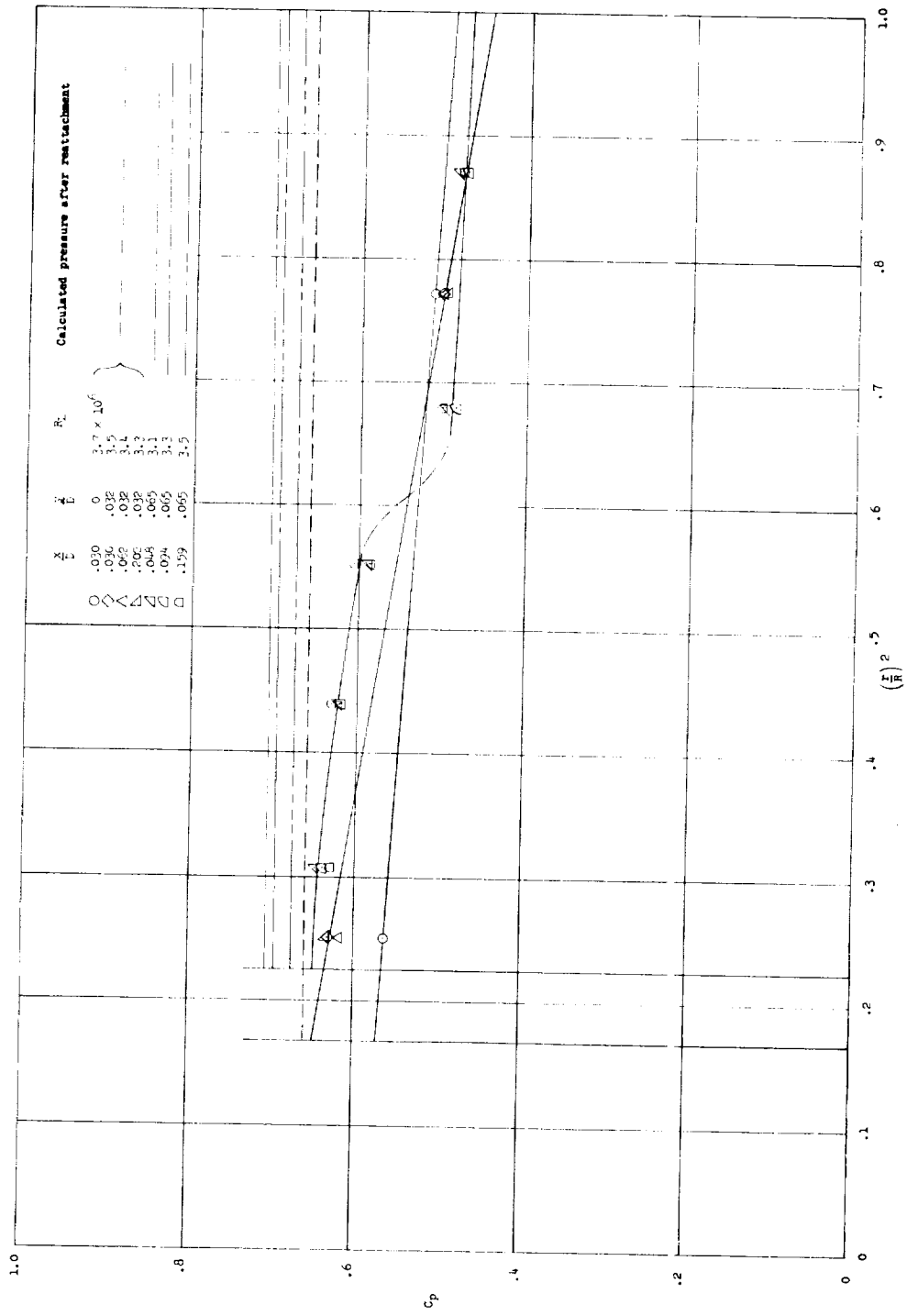

(c) $R_L \approx 3.4 \times 10^6$.

Figure 8.- Continued.

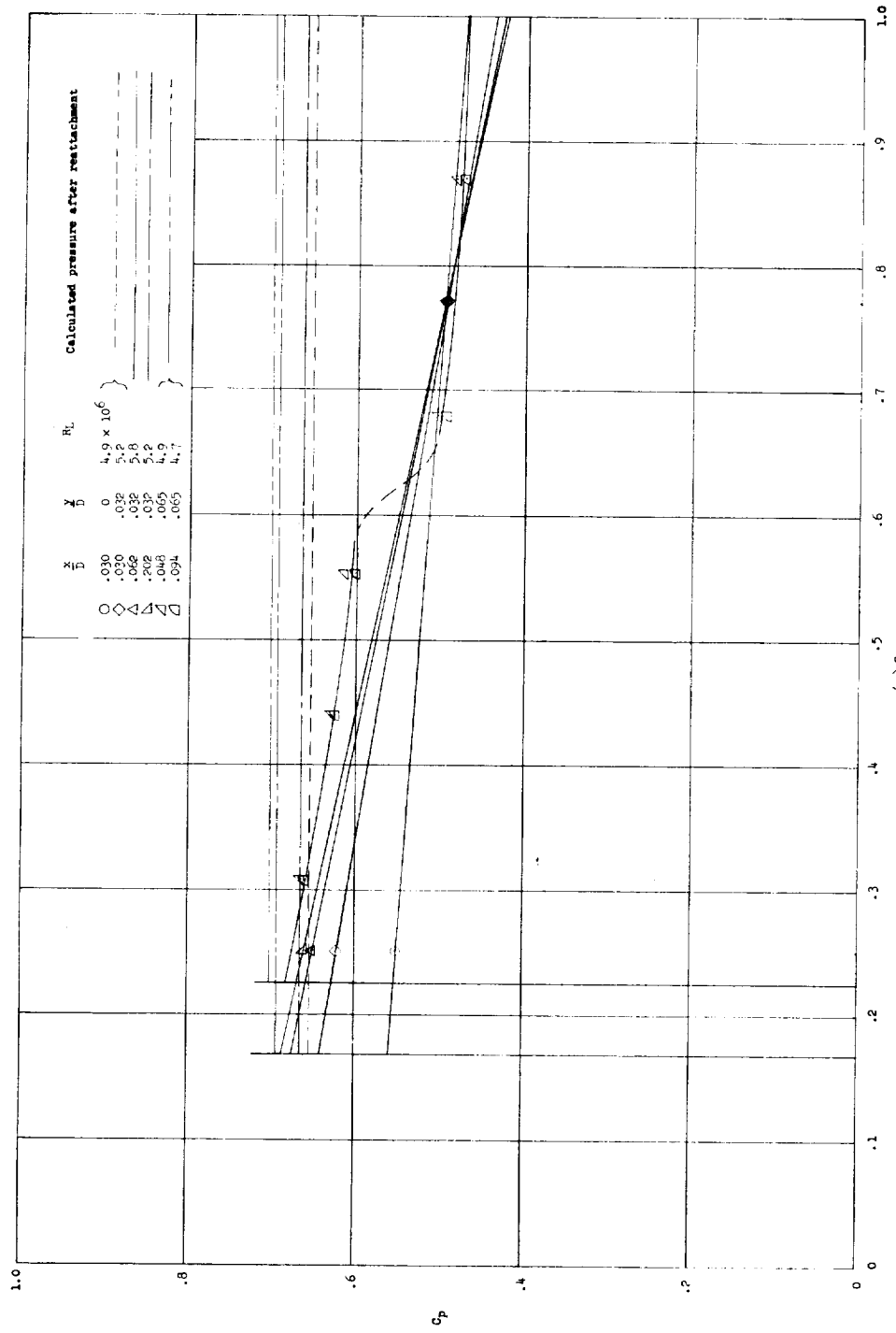

(d) $R_L \approx 5.1 \times 10^6$.

Figure 8.- Continued.

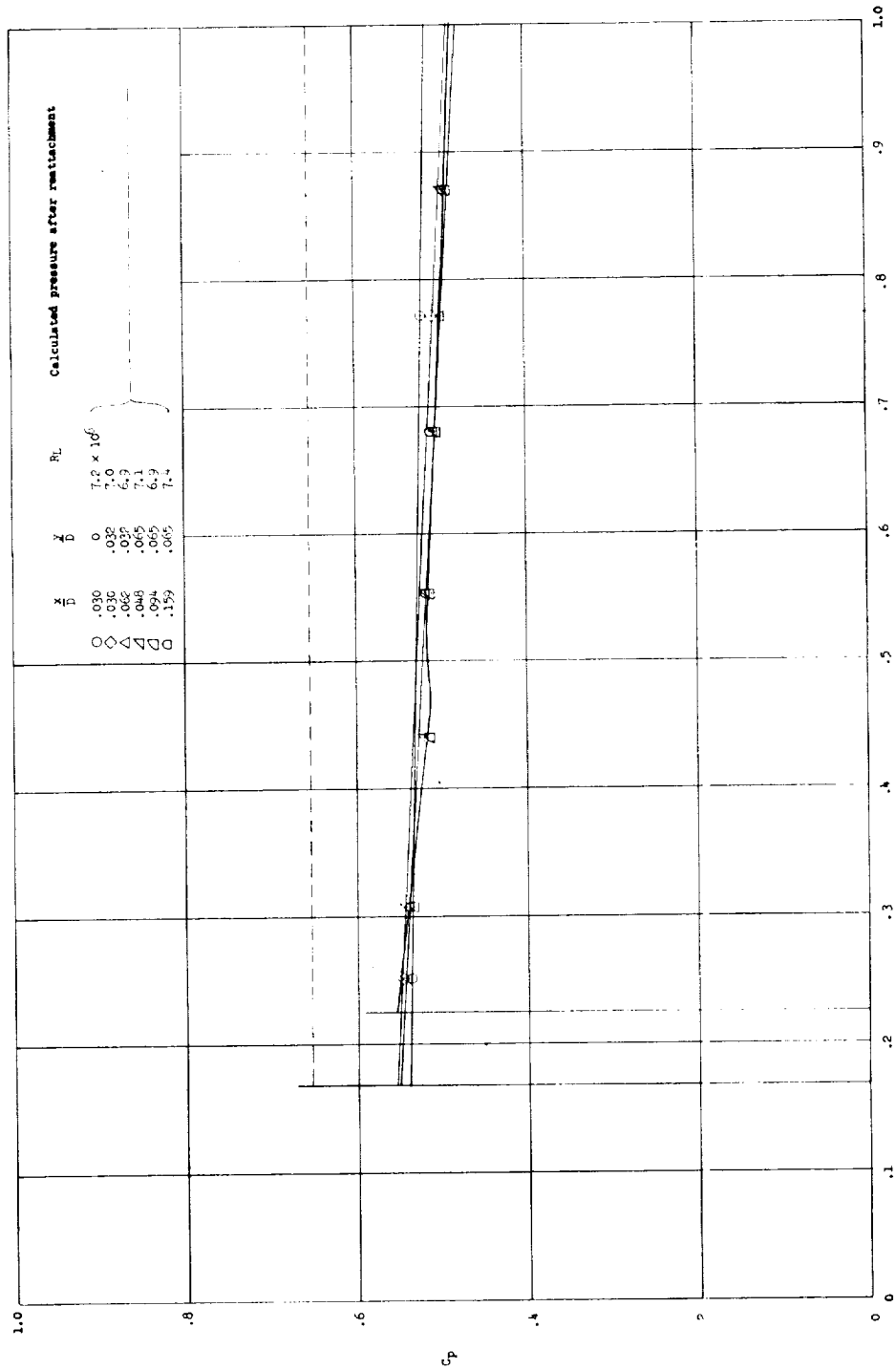

(e) $R_L \approx 7.1 \times 10^6$.

Figure 8.- Concluded.

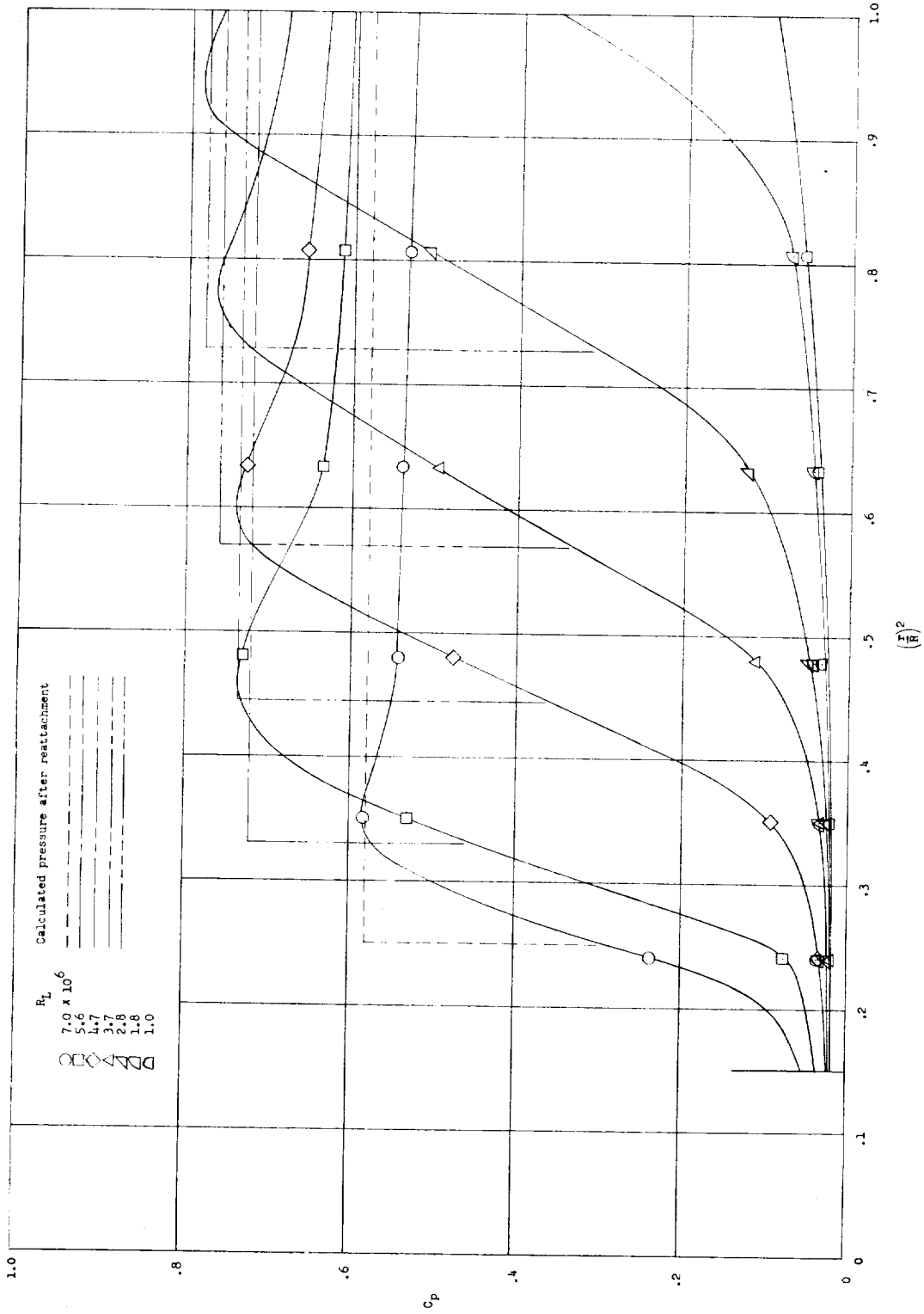

Figure 9.- Experimental and computed pressures on flare with no bleed.

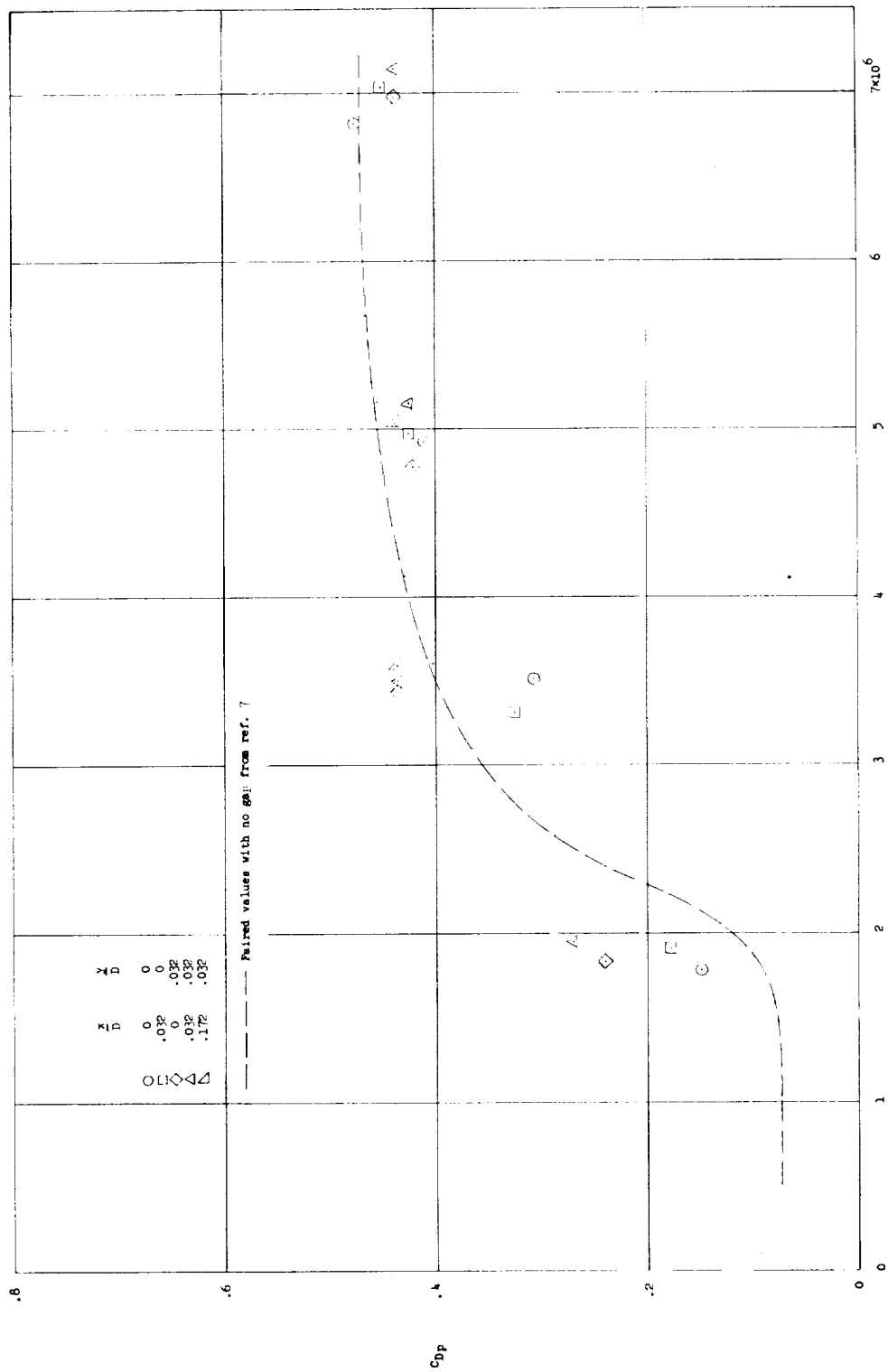

Figure 10.- Integrated pressure drag on sharp-leading-edge flare.

L-1221

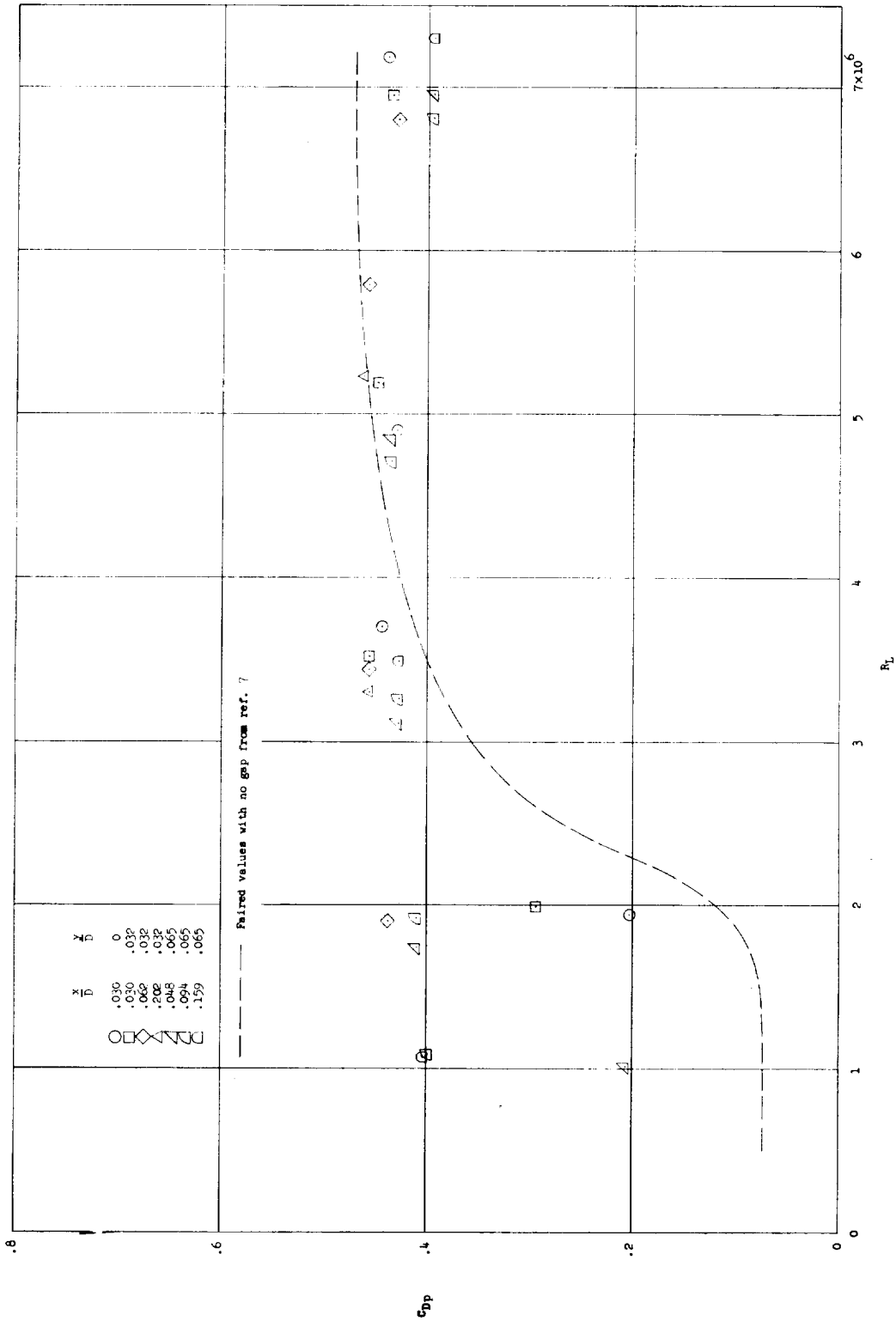

Figure 11.- Integrated pressure drag on blunt-leading-edge flare.

Figure 12.- Heat transfer to sharp-leading-edge flare.

L-1221

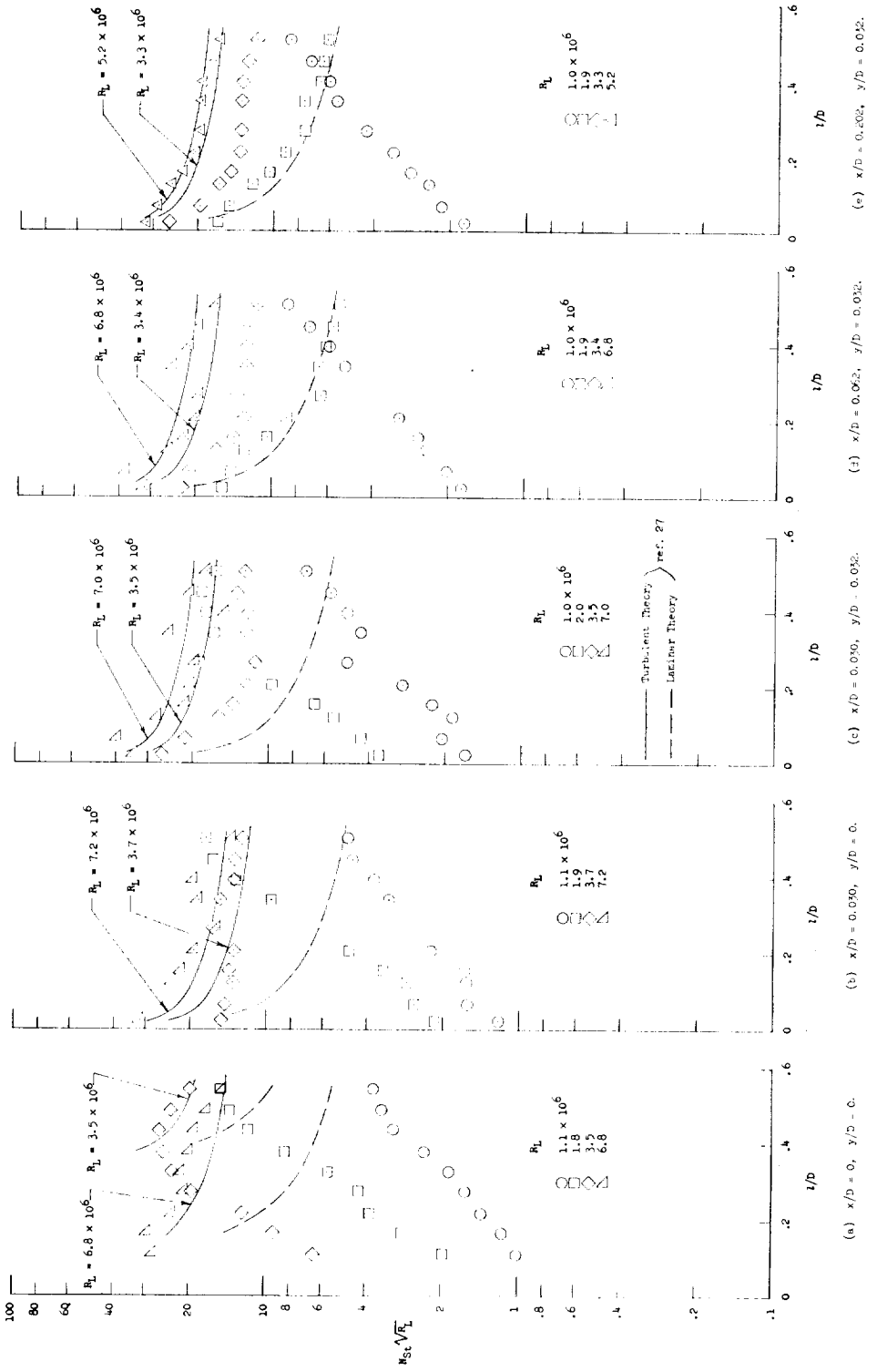

Figure 13.- Heat transfer to blunt-leading-edge flare.

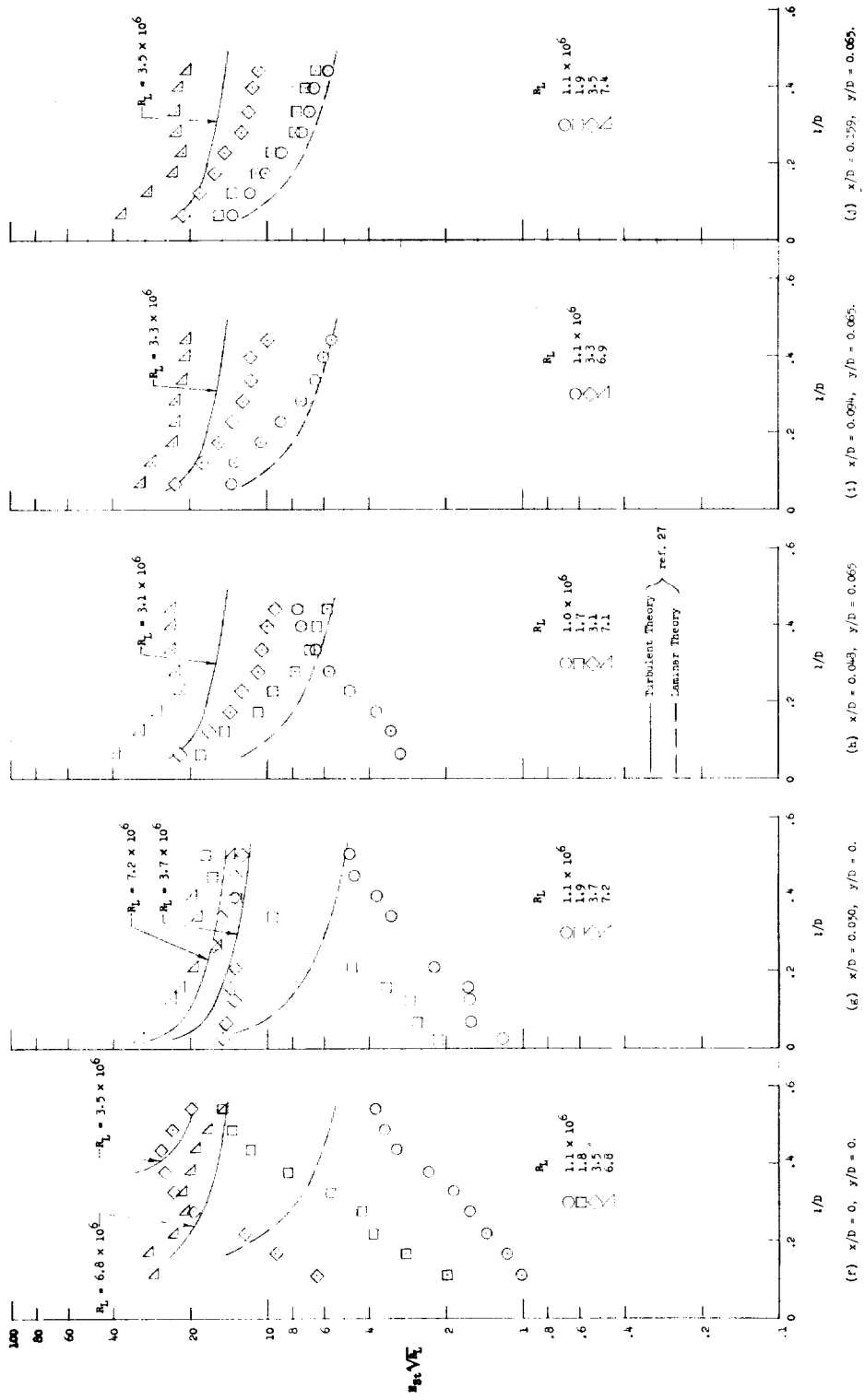

Figure 13.- Concluded.

L-1221

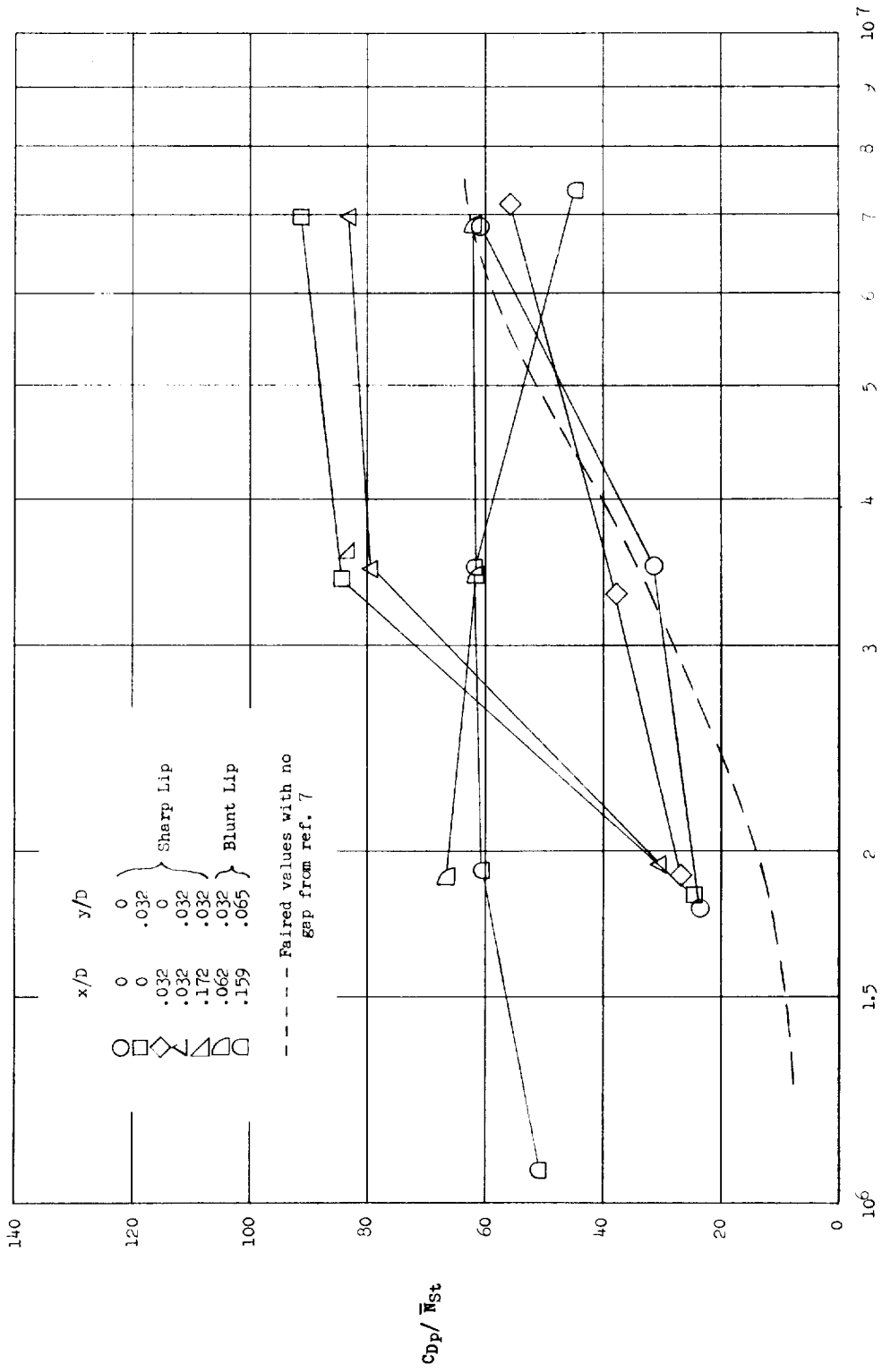

Figure 14.- Ratio of pressure drag coefficient to average heat-transfer coefficient.